3. DATING COEVAL MAFIC MAGMATISM AND ULTRAHIGH-TEMPERATURE METAMORPHISM IN THE ANÁPOLIS-ITAUÇU COMPLEX, CENTRAL BRAZIL

Maria Emilia Schutesky Della Giustina[1]*

Márcio Martins Pimentel[1a]

Cesar Fonseca Ferreira Filho[1]

Maria Helena Bezerra Maia de Hollanda[2]

[1] Universidade de Brasilia, Instituto de Geociencias, 70910-900, Brasilia-DF-Brazil

*Correponding author: maria_emilia@unb.br;

Phone: +55-61-3307-1113; Fax: +55-61-3272-4286

[2] Universidade de São Paulo, Instituto de Geociências, Rua do Lago, 562, Cidade Universitária, 05508-900, São Paulo-SP-Brazil.

Abstract

Dating granulites has always been of great interest because they represent one of the most extreme settings of an orogen. Owing to the resilience of zircon, even in such severe environments, the link between P-T conditions and geological time is possible. However, a challenge to geochronologists is to define whether the growth of new zircon is related to pre- or post-P-T peak conditions and which processes might affect the (re)crystallization. In this context, the Anápolis-Itauçu Complex, a high-grade complex in central Brazil with ultra-high temperature (UHT) granulites, may provide valuable information within this topic.

The Anápolis-Itauçu Complex (AIC) includes ortho- and para-granulites, locally presenting UHT mineral assemblages, with igneous zircon ages varying between 760 and 650 Ma and metamorphic overgrowths dated at around 650-640 Ma. Also common in the Anápolis-Itauçu Complex are layered mafic-ultramafic complexes metamorphosed under high-grade conditions.

This article presents the first geological and geochronological constraints of three of these layered complexes within the AIC, the Damolândia, Taquaral and Goianira-Trindade complexes. U-Pb (LA-

[a] Present address: Universidade Federal do Rio Grande do Sul, Instituto de Geociências, 91501-970, Porto Alegre-RS-Brazil.

ICPMS, SHRIMP and ID-TIMS) zircon analyses reveal a spread of concordant ages spanning within an age interval of ~80 Ma, which suggests an "upper" intercept age of ~670 Ma. Under cathodoluminescence imaging, these crystals show partially preserved primary sector zoning, as well as internal textures typical of alteration during high-grade metamorphism, such as inward-moving boundaries. Zircon grains reveal homogeneous initial $^{176}Hf/^{177}Hf$ values within populations and also in crystal-scale domains in all samples. Moreover, Hf isotopic ratios show correlation neither with U-Pb ages nor with Th/U ratios, suggesting that zircon grains crystallized during a single growth event. It is suggested, therefore, that the observed spread of concordant U-Pb ages may be related to a memory effect due to coupled dissolution-reprecipitation process during high grade metamorphism. Thus, it is unlikely that the emplacement of the mafic-ultramafic complexes and UHT metamorphism in the Anápolis-Itauçu Complex represent unrelated geological episodes.

Therefore, understanding the emplacement and metamorphism of this voluminous mafic magmatism is crucial, given that they may characterize the additional heat source for the development of the ultra-high temperature paragenesis recorded in the paragranulites.

Key-words: Brasília Belt, metamorphic zircon, UHT metamorphism, hot orogen, Hf-in-zircon, coupled dissolution-reprecipitation process

3.1.Introduction

In recent years, petrological studies of granulite terranes have shown that these rocks can experience extreme P-T conditions, which may be substantially more vigorous than previously recognized. The so-called *ultra-high temperature granulites*, recording temperatures higher than 900°C in a moderate pressure environment, are present in most orogens. The origin of these rocks requires extremely hot crustal conditions, which cannot be explained by the numerical models currently available for collisional orogens (Jamieson *et al.*, 1998, 2004; Beaumont *et al.*, 2001, 2006; Collins, 2002) Even considering a large-hot orogen model, when compared to the real geological data there is still a thermal gap of about 100 to 200°C, which requires an additional heat source (Harley, 1998, 2004, 2008). Such supplementary thermal gradient might be found in accretionary orogens (Collins, 2002), where extensional intervals in the overall collisional setting promote lithospheric thinning and, consequently, the ascent of hot asthenospheric mantle generating elevated heat flow (Schott & Schmeling, 1998). This process

results in extensive mafic magmatism associated in space and time with high-temperature-low-pressure metamorphism (Sandiford & Powell, 1986; Schott & Schmeling, 1998).

In central Brazil, such scenario may be recognized in the Anápolis-Itauçu Complex (AIC), which represents the metamorphic nucleus of the Brasilia Belt. The geological framework, with UHT occurrences spatially associated with mafic granulites, suggests that the Brasilia Belt may correspond to a large, hot orogen, as suggested before (Pimentel *et al.*; 2003; Giustina *et al.*, 2009).

Previous studies combining geological and geochronological aspects of the UHT paragranulites of the AIC reveal the age of ~645 Ma for the peak of metamorphism (Moraes *et al.*, 2002; Piuzana *et al.*, 2003a; Baldwin & Brown, 2008). However, associated mafic complexes have never been the topic of such kind of research. The data available for the regional mafic magmatic event in the Brasilia Belt is limited to the arc terranes, exposed to the west of the AIC.

Therefore, this study aims at describing the geology of three layered mafic-ultramafic complexes, occurring within the Anápolis-Itauçu Complex, as well as discuss their isotopic and geochronological record, in order to verify the relationship between mafic magmatism and metamorphism in the AIC. Mafic intrusions emplaced into deep crustal levels represent the most suitable rock association for this study. The intrusions investigated here present partially preserved igneous textures and high-grade metamorphic imprint.

3.2. Geological setting

The Brasília Belt is a Neoproterozoic orogen in central Brazil, developed throughout island arc amalgamation and continental collision between the São Francisco-Congo and the Paranapanema continent to the south, covered by the Paraná Basin (Figure 3.1; Pimentel et al., 2000; Valeriano et al., 2008). It is part of a global network of Neoproterozoic orogenic belts which resulted in the final amalgamation of Gondwana. It may be divided into four domains: (i) in the easternmost part is a thrust-and-fold belt consisting of various Neoproterozoic metasedimentary sequences formed along the western margin of the São Francisco Craton, (ii) in the central part of the belt, the metamorphic core is exposed, comprising high-grade rocks and ultra-high temperature granulites – the Anápolis-Itauçu Complex, (iii) the Goiás Massif, interpreted as a microcontinent/exotic terrane accreted to the orogen at the end of the Neoproterozoic, and (iv) the Goiás Magmatic Arc, which represents a juvenile terrane forming

the westernmost part of the belt (Brito Neves & Cordani, 1991; Pimentel & Fuck, 1992; Fuck *et al.*, 1994; Pimentel *et al.* 2000; Figure 3.1A).

The Anápolis-Itauçu Complex (AIC) is located in the southern branch of the Brasília Belt (Figure 3.1B). It constitutes an elongated NW-SE zone of high-grade rocks exposed between the Goiás Magmatic Arc and lower-grade Neoproterozoic Araxá Group micaschists and quartzites. Geological contacts are marked by high-angle shear-zones, thus preventing the identification of clear stratigraphic or cross-cutting relationships between the different rock units. However, geochronological data support the interpretation that at least part of the AIC may represent high-grade equivalents of the Araxá Group (Piuzana *et al.*, 2003b) and, moreover, it might be an exposure of the root of the original mountain chain.

The AIC includes a variety of rock-types forming NW-oriented segment, in which three main rock associations may be recognized. The orthogranulites are represented by tonalitic to granodioritic gneisses, as well as by mafic rocks, exposed either as dioritic/gabbroic granulites or as mafic-ultramafic complexes. Such layered bodies are composed of peridotite, pyroxenite, gabbro and gabbro-anorthosite. Relict igneous textures and layering are usually observed. However, these complexes are often strongly foliated and metamorphosed under amphibolite to granulite facies conditions. Geochemical analysis point toward a tholeiitic parental magma, with LREE enrichment and a negative Eu anomaly, and the high-Al content of relict igneous pyroxenes suggests that the intrusion took place at deep levels in the crust (Silva, 1991, 1997; Nilson, 1992).

Example of these layered bodies are the Damolândia, Taquaral (Silva, 1997), Goianira-Trindade (Nilson & Motta, 1969) and Águas Claras complexes (Nilson, 1992), which are interpreted to be coeval with those exposed to the west, within the Goiás Magmatic Arc domain (Laux *et al.*, 2004).

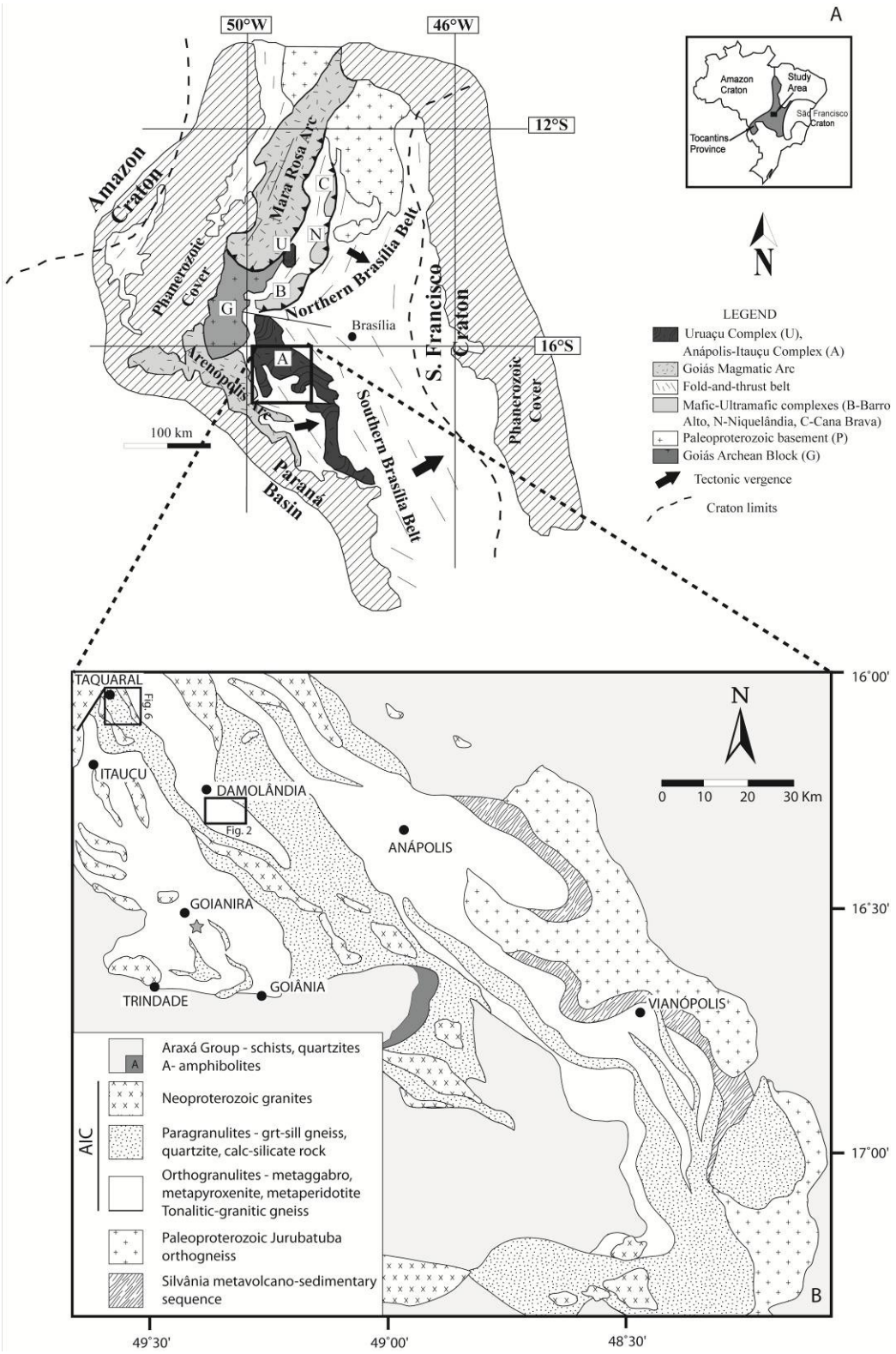

Figure 3.1 - A) Regional sketch map of the Brasilia Belt, in the eastern part of the Tocantins Province (modified from Giustina *et al.*, 2009). B) Geological map of the central part of the Anápolis-Itauçu Complex (modified from Piuzana *et al.*, 2003). The star represents the location of sample INHO-01.

Metasedimentary rocks are typically represented by aluminous granulites with variable amounts of sillimanite, garnet, spinel, cordierite and feldspars. Commonly, these rocks occur as massive outcrops or either form bands in stromatic migmatites, in which fine-grained mafic granulites, interpreted as metabasalts, are also observed (Winge, 1995). Calc-silicate rocks and impure quartzites are also recognized. Ultrahigh-temperature mineral assemblages, such as saphirine+quartz, orthopyroxene+sillimanite+quartz, wollastonite+scapolite and hercynite+quartz have been identified in several localities of the AIC (Moraes *et al.*, 2002, 2007; Baldwin *et al.*, 2005). The paragranulites preserve composite P-T paths, with a first near-isothermal decompressional phase, when the thermal peak is achieved, which is followed by a near-isobaric cooling stage (Moraes *et al.*, 2002; Baldwin & Brown, 2008).

A large number of granites also constitute the AIC (Figure 3.1B). They show variably deformational and metamorphic overprint, achieving even granulite facies conditions. Most of these granitic rocks are peraluminous and the Nd isotopic signature indicates that they may be the melting products of either the aluminous paragranulites of the AIC or metasedimentary rocks of the Araxá Group (Piuzana *et al.*, 2003a). In some of these bodies U-Pb ages for zircon igneous cores and metamorphic rims are identical and, therefore, the granites may be interpreted as representative of deep-crustal, syn-tectonic intrusions (Piuzana *et al.*, 2003a).

SHRIMP U-Pb ages of igneous zircon from felsic orthogranulites vary between 760 and 650 Ma and metamorphic overgrowths are dated at 650-640 Ma (Piuzana *et al.*, 2003a). T_{DM} Sm-Nd model ages of granulitic rocks fall into two age intervals, between 2.3-1.9 Ga and 1.7-1.4 Ga, and ε_{Nd} (T) values are negative, ranging from -9.3 to -1.4 (Piuzana *et al.*, 2003a). The younger T_{DM} values are in agreement with the zircon inheritance pattern observed in paragranulites (2.0 to 0.8 Ga). Both the Nd and the U-Pb data indicate an important Neoproterozoic sedimentary source.

3.3. Damolândia and Taquaral Layered Complexes

The Damolândia and Taquaral layered mafic-ultramafic complexes occurs within high-grade gneiss and granulites from the AIC. Both layered complexes were overprinted by heterogeneous high-grade metamorphism and associated tectonism. While primary igneous textures and mineralogy are largely preserved in rocks of the EW trending Damolândia Complex,

such features are just locally preserved in the NNW trending Taquaral Complex, which consists mainly of highly foliated and recrystallized mafic-ultramafic rocks.

Damolândia

The Damolândia Complex is a poorly exposed medium-size (ca 15 km^2) layered intrusion. Extensive mapping and mineral exploration data developed by International Nickel Venture Ltd. in 2006-2008 provided constraints on the geology and stratigraphy of the layered sequence (Figure 3.2). The host rocks of the Damolândia Complex were not investigated in detail, but regional mapping indicates that they consist mainly of basic to intermediate granulite in the north, and highly foliated leptynite[b] and felsic gneiss in the south (Figure 3.2). Mafic-ultramafic rocks of the Damolândia Complex form irregular domains of interlayered peridotite-pyroxenite-norite associated with domains of mafic rocks, mainly norite and gabbronorite, and domains where medium to coarse-grained diorite occur. Due to poor exposition of mafic and ultramafic rocks, the mapped domains are based on soil characteristics (Figure 3.3A) supported by scattered outcrops (Figure 3.3B) and soil geochemistry surveys. Layered rocks of the Damolândia Complex are heterogeneously tectonized and recrystallized in discrete zones, where primary igneous rocks were transformed into highly foliated mafic or ultramafic granulites.

Extensive drilling developed in the southwestern portion of the Damolândia Complex expose complete sections of the interlayered peridotite-pyroxenite-norite domain. A representative drill hole from this domain consists of a ca 200 meter-thick sequence of ultramafic cumulates within mafic cumulates (Figure 3.4). The facing of the layered sequence is not constrained by primary structures, but layering in the core defined by aligned prismatic pyroxenes indicates steep dip to the north. Norite and gabbronorite are orthopyroxene and plagioclase cumulates, with variable amounts of intercumulus clinopyroxene, hornblende and minor phlogopite. Pyroxenite consists of cumulus orthopyroxene, or orthopyroxene and chromite (ca 1-3 vol. %), with variable amounts of intercumulus plagioclase, clinopyroxene, hornblende and minor phlogopite. Textures of pyroxenite vary from medium- to coarse-grained adcumulate (orthopyroxenite), to mesocumulate and orthocumulates (usually websterite or melanorite). The transition from pyroxenite to norite is gradational and characterized by the increase of interstitial

[b] Leptynites are fine-grained leucocratic sill-grt gneisses with a granoblastic texture, probably of granitic nature (Winge & Danni, 1994).

plagioclase. Cyclic interlayering of peridotite (mainly harzburgite) and pyroxenite characterizes the central zone of ultramafic cumulates in drill hole FSDM-07 (Figure 3.4). Peridotite (Figure 3.3C and 3.3D) is an olivine and chromite (ca 1-3 vol. %) cumulate with variable amounts of intercumulus orthopyroxene and minor clinopyroxene, hornblende, plagioclase and phlogopite. Interlayered peridotite and pyroxenite form up to dozen of meter-thick layers with sharp contacts, splitting the ultramafic samples into one group of olivine-rich peridotite (MgO > 27 wt. %) and another of pyroxenite (MgO < 17 wt. %). Few discordant bodies of coarse-grained hornblende-bearing gabbronorite or hornblende diorite (Figure 3.3F) occur throughout the layered sequence. These bodies are usually few meter-wide and have accessory ilmenite, apatite and zircon, suggesting their crystallization from evolved magmas, possibly resulting from residual trapped liquids.

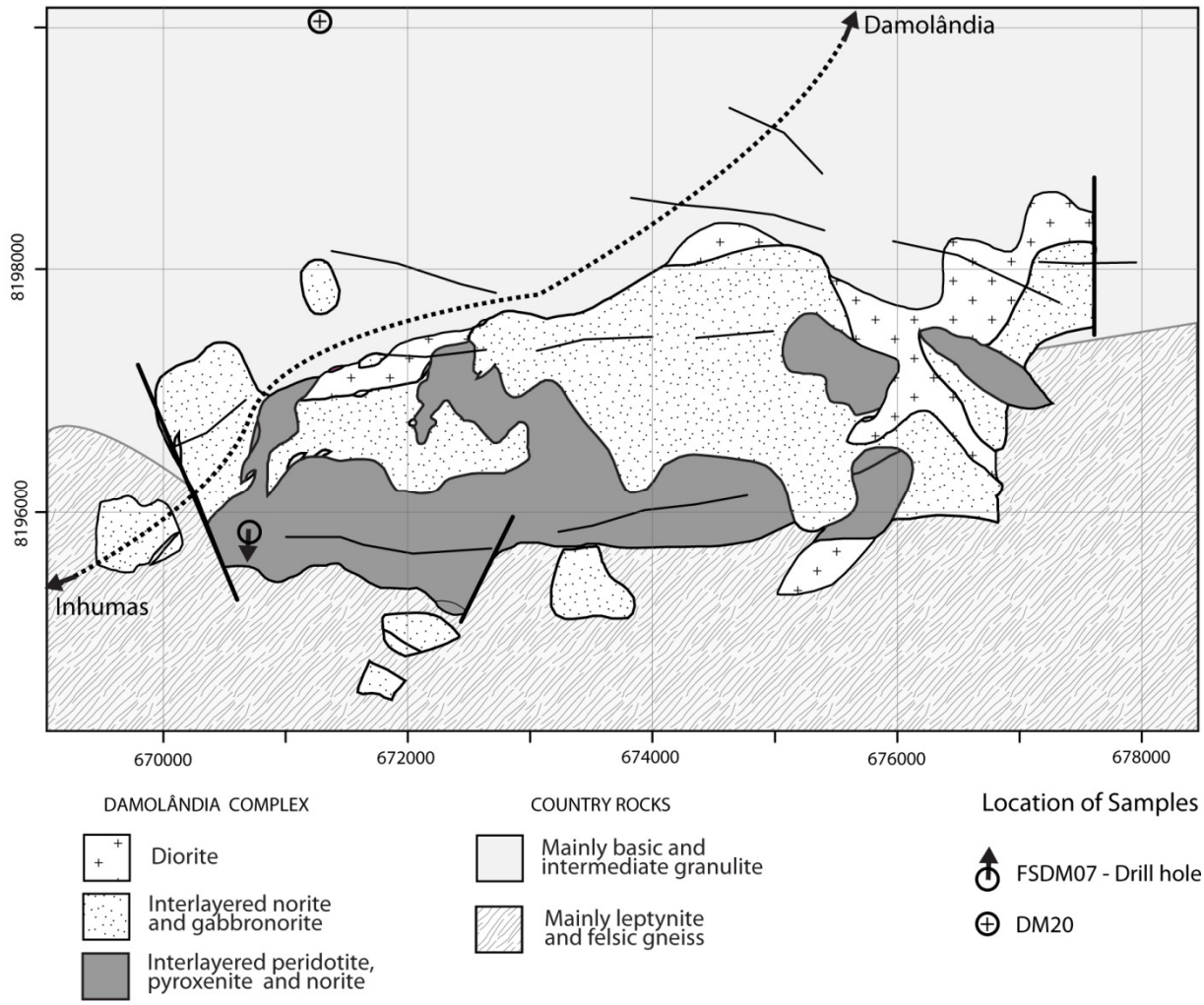

Figure 3.2 - Geology of the Damolândia Complex (from unpublished report of International Nickel Venture Ltd.).

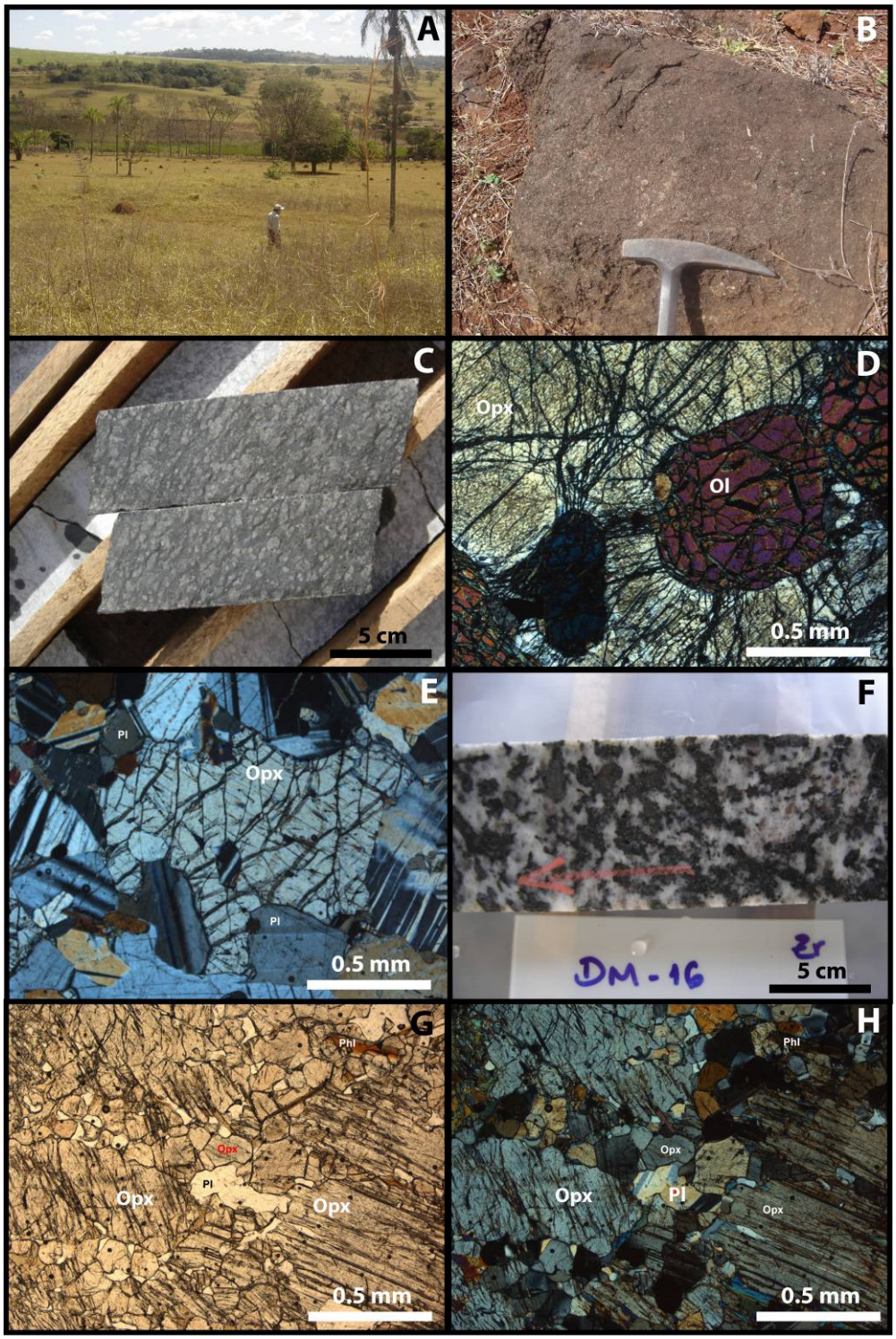

Figure 3.3 - A) View of the area close to the drill hole FSDM-07. Rare outcrops and abundant dark brownish termite mounts developed on soil from ultramafic rocks (close to drill hole FSDM-07). B) Orthopyroxenite with interstitial white plagioclase (close to drill hole FSDM-07). C) Harzburgite from drill hole FSDM-07. D) Photomicrograph of harzburgite consisting of cumulus olivine (Ol) enclosed in large orthopyroxene oikocryst (opx). E) Photomicrograph of norite consisting of cumulus orthopyroxene (opx) and plagioclase (Pl). F) Zircon-bearing hornblende gabbronorite. Sample DM-16 from drill hole FSDM-07. G) and H) Photomicrograph of partially recrystallized plagioclase-bearing orthopyroxenite. Large igneous orthopyroxene crystals are recrystallized into fine-grained granoblastic aggregates.

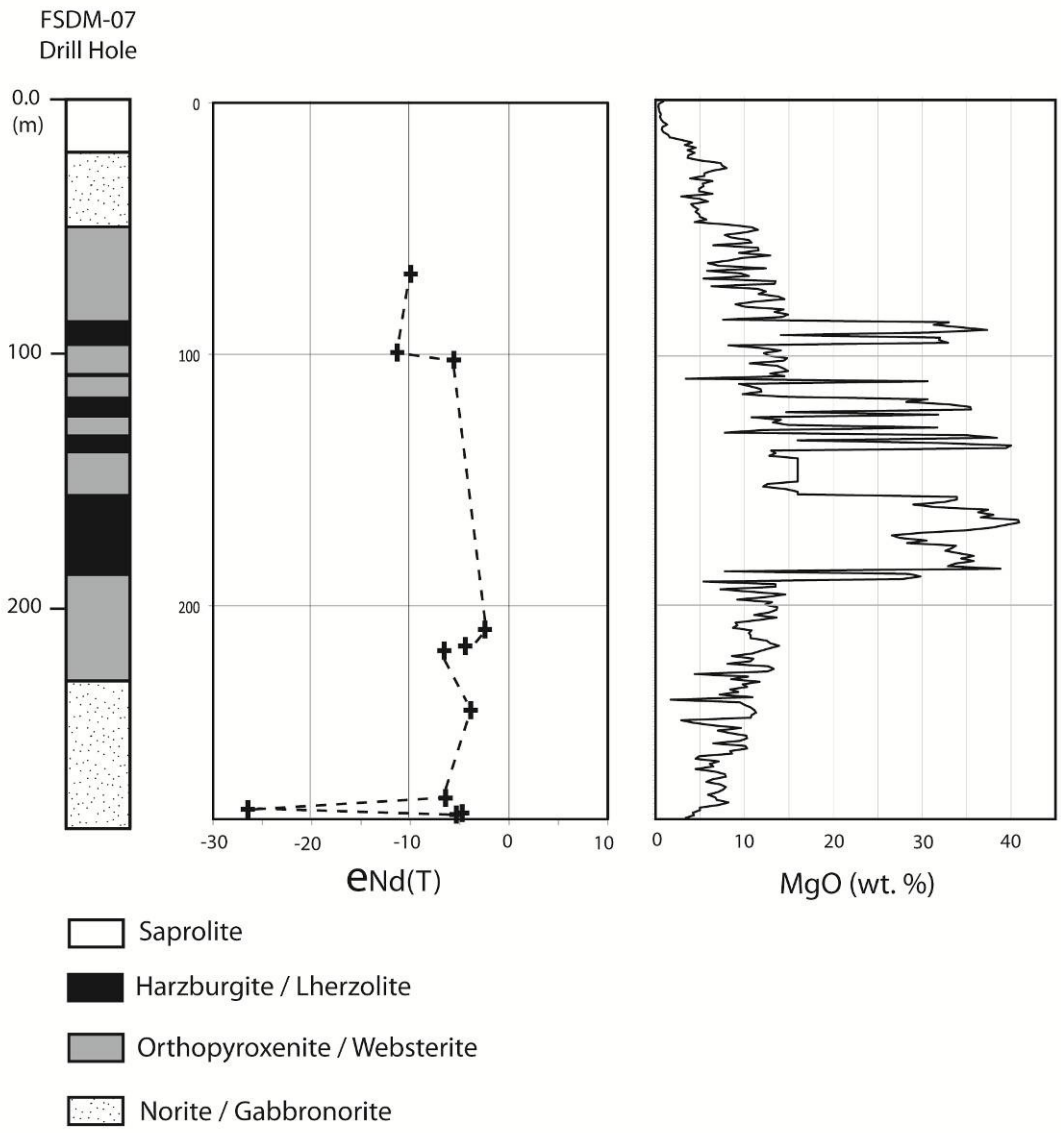

Figure 3.4 - Log, MgO content and εNd(T) for drill hole FSDM-07.

Cumulus minerals in the layered rocks suggest that the sequence of crystallization in the Damolândia Complex consists of olivine+chromite, orthopyroxene+chromite, orthopyroxene, orthopyroxene+plagioclase and orthopyroxe+plagioclase+clinopyroxene. The crystallization sequence described for the Damolândia Complex is very common (e.g. Bushveld Complex; Serra da Onça). The correlation of MgO content with CaO, TiO_2, K_2O and Cr for layered rocks of the drill hole FSDM-07 (Fig. 3.5) is consistent with this sequence of crystallization of cumulus minerals. High MgO contents of peridotite samples (up to 41 wt. %) suggests high MgO content of olivine. Low CaO and TiO_2 contents are consistent with the predominance of orthopyroxene

over clinopyroxene in the layered rocks, while high Cr contents are consistent with the presence of chromite in both peridotite and pyroxenite samples. Scattered high contents of K_2O are associated with disseminated interstitial phlogopite. High K_2O contents show no correlation with MgO content suggesting that they result from inhomogeneous assimilation of crustal rocks by the parental magma.

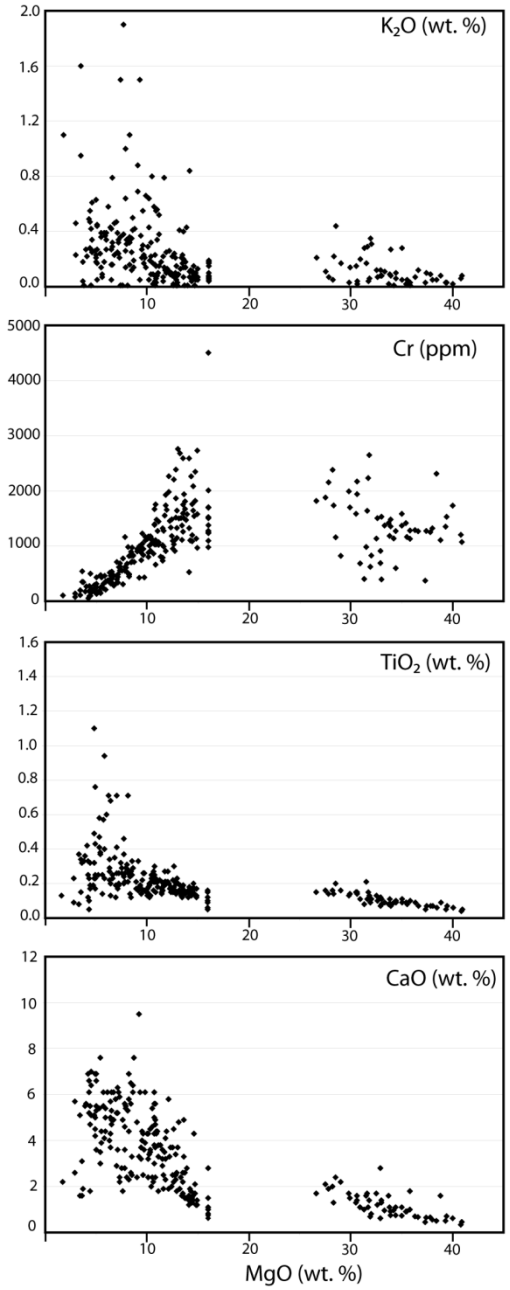

Figure 3.5 - Plot of MgO versus CaO, TiO_2, Cr and K_2O for the drill hole FSDM07.

Primary igneous texture and mineralogy prevail throughout the layered sequence of the drill hole FSDM-07. Recrystallization and ductile deformation are restricted to few-meter wide discrete zones. In these zones the primary igneous mineralogy is partially (Figure 3.3G and 3.3H) to completely recrystallized into fine-grained granoblastic assemblages of metamorphic minerals. Recrystallized norite and gabbronorite consist of fine-grained granoblastic aggregates of plagioclase, orthopyroxene, clinopyroxene and dark-brown amphibole. This assemblage indicates that recrystallization occurred under conditions of high temperature (equivalent to the granulite facies of regional metamorphism).

Taquaral

The Taquaral Complex was considered by Silva (1997) as a large (up to 50 km-long) layered mafic-ultramafic complex submitted to high-grade metamorphism and associated tectonism. Silva (1997) proposed a stratigraphic column with 5 km of inferred thickness for the Taquaral Complex. However, extensive exploration developed by mining companies in the Taquaral Complex indicates that it consists of several elongated small to medium-size (up to 15 km-long) highly tectonized mafic and mafic-ultramafic bodies. Stratigraphic correlations between different bodies are unconstrained and the complex should be considered by now as a cluster of NNW trending mafic and mafic-ultramafic bodies. Detailed mapping supported by exploration data was developed by International Nickel Venture Ltd. in 2007-2008 in the northern segment of the Taquaral Complex. Results indicate the existence of several small to medium-size mafic-ultramafic bodies (Figure 3.6) surrounded by high-grade felsic gneiss and leptynite. Mapped mafic and ultramafic rocks of the Taquaral Complex are highly tectonized and recrystallized. They have pervasive tectonic foliation (Figure 3.7A and 3.7B) parallel with the NNW (subvertical to SW dip) trend of host rocks.

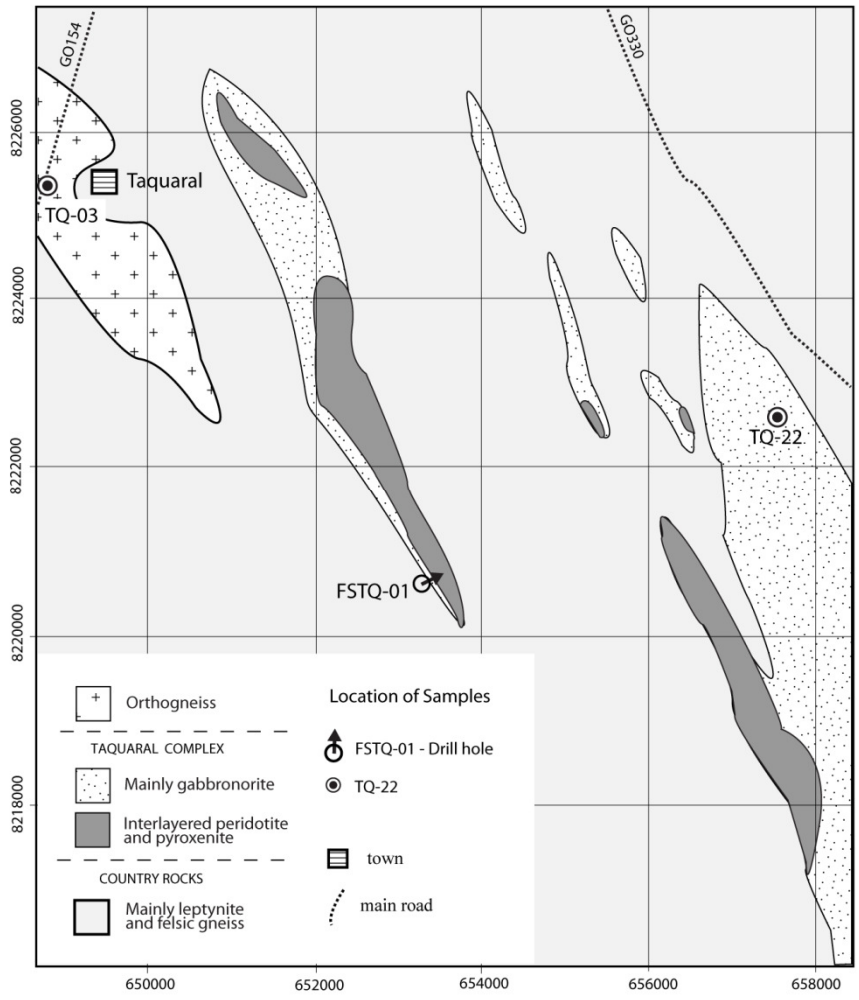

Figure 3.6 - Geology of the northern area of the Taquaral Complex (from unpublished report of International Nickel Venture Ltd.).

Cumulus minerals in the layered rocks suggest that the sequence of crystallization in the FSTQ-01 drill core consists of olivine + chromite, orthopyroxene + chromite, orthopyroxene + clinopyroxene, orthopyroxene + clinopyroxene +plagioclase and orthopyroxene + clinopyroxene + plagioclase + ilmenite. This crystallization sequence is different from the Damolândia Complex, indicating an early cristallization of clinopyroxene in the Taquaral Complex. The crystallization sequence described for the Taquaral Complex is similar to what is described in the Great Dyke and in the Niquelândia Complex (Ferreira Filho *et al.*, 1998). The correlation of MgO content with CaO, TiO_2, K_2O and Cr for layered rocks of the drill hole FSTQ-01 (Figure 3.9) is consistent with this sequence of crystallization of cumulus minerals.

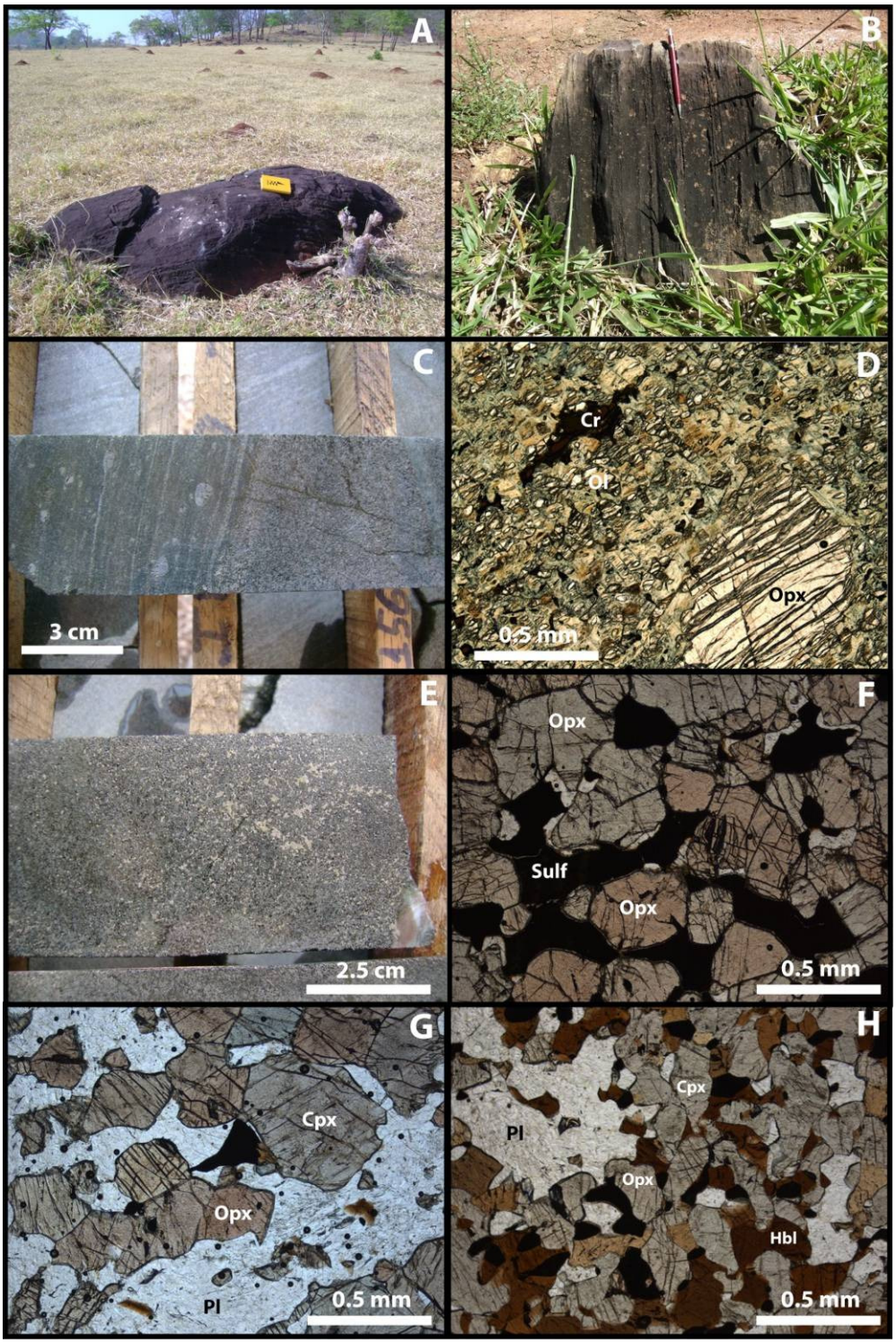

Figure 3.7 - A) Boulder of highly foliated mafic granulite. The mineral assemblage consists of orthopyroxene, clinopyroxene, plagioclase, hornblende and magnetite. Abundant reddish termite mounts are developed on soil from mafic rocks (locality of sample TQ-22). B) Outcrop of highly foliated subvertical peridotite. Elongated pyroxene crystals and pyroxene aggregates become evident in the weathered surface. C) Sharp contact between peridotite (left side) and pyroxenite (right side) from drill core FSTQ-01. Large pyroxene crystals in the peridotite show up in lighter colors. D) Photomicrograph of peridotite consisting of partially serpentinized olivine crystals (Ol) associated with large orthopyroxene (opx) and chromite (Cr). E) Orthopyroxenite with interstitial sulfides from drill core FSTQ-01.

Cont. Figure 3.7 - F) Photomicrograph of orthopyroxenite consisting of cumulus orthopyroxene (opx) and interstitial sulfides (Sulf) and plagioclase (white and low relief minerals) G) Photomicrograph of gabbronorite from FSTQ-01. Ilmenite (opaque) and phlogopite (small brownish lamellae) are accessory minerals. H) Photomicrograph of recrystallized mafic rock from drill hole FSTQ-01. This sample is a mafic granulite with fine-grained granoblastic texture. The mineral assemblage consists of orthopyroxene (Opx), clinopyroxene (Cpx), brownish hornblende (Hbl), plagioclase (Pl), ilmenite (opaques) and spinel (small greenish crystals associated with ilmenite).

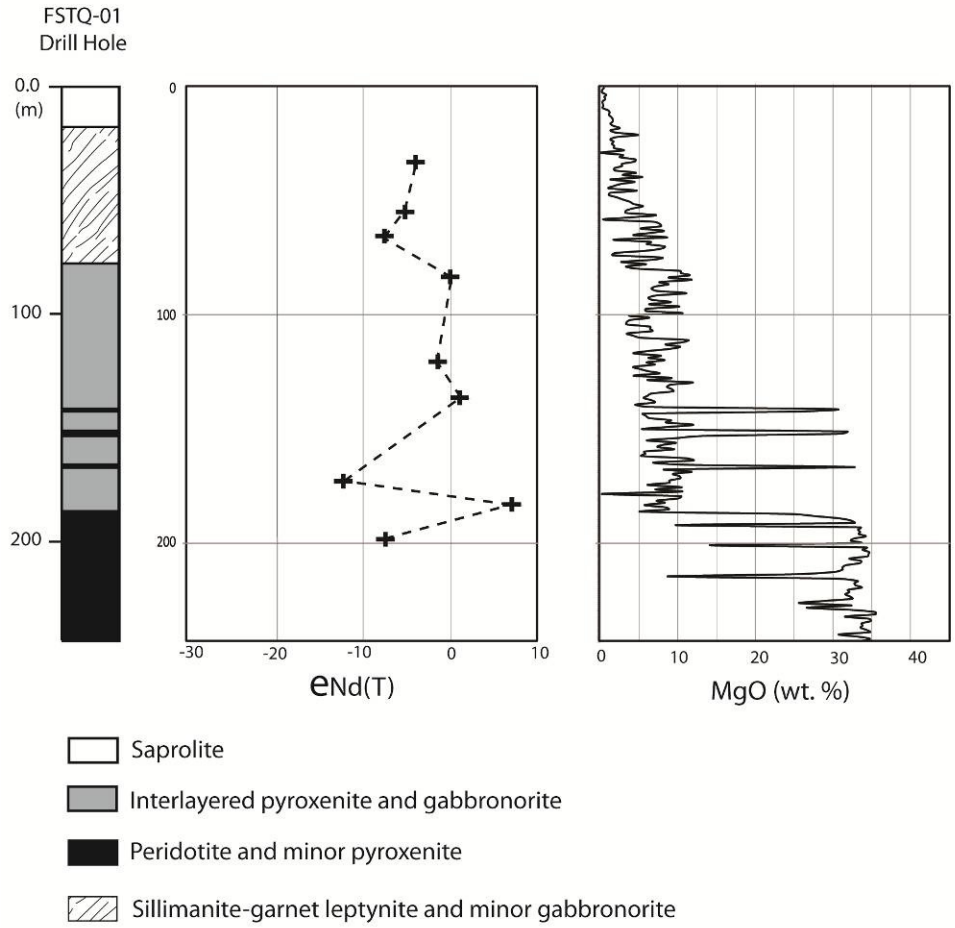

Figure 3.8 - Log, MgO content and εNd(T) for drill hole FSTQ-01 (see Fig. 6 for location).

Samples of peridotite (MgO > 24 wt.%) and pyroxenite-gabbronorite (MgO < 15 wt.%) form two distinct groups, indicating the sharp contact between olivine-rich peridotite and pyroxenite, as well as the gradational transition between pyroxenite and gabbronorite. High MgO contents of peridotite samples (up to 35 wt. %) are consistent with high MgO content of olivine from peridotite (up to Fo90) reported from Silva (1997). Higher CaO and TiO_2 contents, when compared to data from the Damolândia Complex, are consistent with the abundance of clinopyroxene in the layered rocks, while high Cr contents are consistent with the presence of

chromite in both peridotite and pyroxenite. Higher CaO contents are particularly significant in peridotites, indicating the abundance of lherzolite in the Taquaral Complex, while harzburgite predominates in the Damolândia Complex. Higher Ti contents in gabbronorite of the Taquaral Complex is associated with disseminated ilmenite. Scattered high contents of K_2O are associated with disseminated interstitial phlogopite. Similar to what was described for the Damolândia Complex, high K_2O contents show no correlation with MgO content suggesting that they result from inhomogeneous assimilation of crustal rocks by the parental magma.

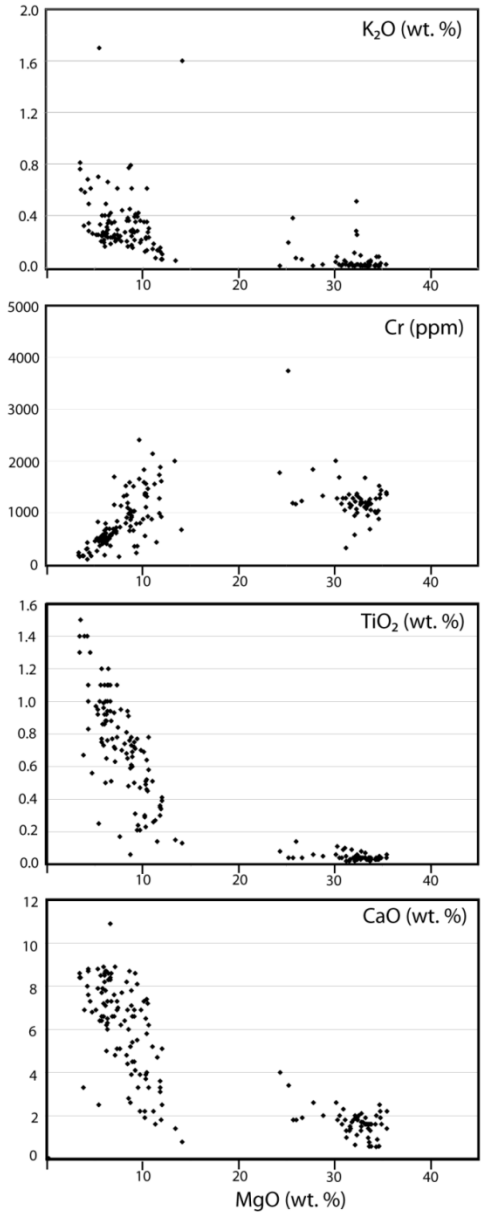

Figure 3.9 - Plot of MgO versus CaO, TiO_2, Cr and K_2O for the drill hole FSTQ-01.

Rocks with metamorphic mineralogy and tectonic texture prevail throughout the layered sequence of drill core FSTQ-01. In these zones the primary igneous mineralogy is recrystallized into fine-grained metamorphic minerals. Recrystallized mafic rocks consist of fine-grained granoblastic aggegates of plagioclase, orthopyroxene, clinopyroxene, dark-brown amphibole and minor spinel (Figure 3.7H), indicating that recrystallization occurred under conditions of high temperature (granulite facies of regional metamorphism). Mafic rocks associated with silimanite-garnet leptynite in the upper part of the drill core are similar to highly tectonized gabbronorite of the layered sequence. This feature suggests that they represent disrupted fragments of the layered sequence.

An elongated body of coarse-grained porphyritic orthogneiss occurs in the northwestern corner of the area investigated by INV (Figure 3.6). This orthogneiss has granitic composition and was sampled for isotopic studies (sample TQ-03).

3.4.Methods

***In situ* zircon analyses**

Zircon concentrates were extracted from ca. 10 kg rock samples using conventional gravimetric and magnetic techniques at the Geochronology Laboratory of the University of Brasília. Mineral fractions were hand-picked under a binocular microscope to obtain fractions of similar size, shape and color. For *in situ* U-Pb and Hf analyses, hand-picked zircon grains were mounted in epoxy blocks and polished to obtain a smooth surface. Backscattered electron and cathodoluminescence images were obtained in order to investigate the internal structures of the zircon crystals prior to analysis.

Before LA-ICP-MS analyses, mounts were cleaned with dilute (ca. 2%) HNO_3. The samples were mounted in an especially adapted laser cell and loaded into a New Wave UP213 Nd:YAG laser (λ = 213 nm), linked to a Thermo Finnigan Neptune Multi-collector ICPMS. Helium was used as the carrier gas and mixed with argon before entering the ICP. The laser was run at a frequency of 10 Hz and energy of ~100 mJ/cm^2 with a spot of 30μm for U-Pb systematics and 40μm for Hf isotopic analyses.

The U-Pb and Hf LA-ICPMS analyses followed the analytical procedure described by Buhn *et al.* (2009) and Matteini *et al.* (2009), respectively, and were performed at the Geochronology Laboratory of the University of Brasília.

Two international zircon standards were analyzed throughout the U-Pb LA-ICPMS analyses. Zircon standard GJ-1 (Jackson *et al.*, 2004) was used as the primary reference material in a standard-sample bracketing method, accounting for mass bias and drift correction. The resulting correction factor for each sample analysis considers the relative position of each analysis within the sequence of 4 samples bracketed by two standard and two blank analyses each (Albarède *et al.*, 2004). The Temora 2 standard (Black *et al.*, 2004) was run at the start and at the end of each analytical session, yielding accuracy around 2% and a precision in the range of 1% (1σ). The errors of sample analyses were propagated by quadratic addition of the external uncertainty observed for the standards to the reproducibility and within-run precision of each unknown analysis. Zircon grains with $^{206}Pb/^{204}Pb$ lower than 1000 were rejected. Plotting of U–Pb data and age calculations were performed using ISOPLOT version 3.0 (Ludwig, 2003) and errors for isotopic ratios are presented at the 1σ level.

Hf isotopic measurements were carried out on zircon grains previously investigated by U-Pb systematics. Only concordant grains (± 5%) were selected. The Hf spot analyses were located in the same CL region of zircon grains and, whenever possible, just on top of the U-Pb analytical pit. Before the laser ablation analyses, JMC 475 standard solution, doped with Yb (Yb/Hf=0.02), was run, yielding a mean $^{176}Hf/^{177}Hf$ ratio of 0.282171±20 (n=4) which is in agreement with values reported in the literature (e.g. 0.282163 +/- 09; Blichert-Toft et. al (1997)). During *in situ* analytical session, GJ-1 zircon (Jackson *et al.*, 2004) was monitored as a reference material and rendered an average $^{176}Hf/^{177}Hf$ value of 0.282001±21 (n=10) in agreement with Zeh *et al.* (2007; 0.282003 +/- 15), Morel *et al.* (2008; 0.282000 +/- 05) and Xie *et al.* (2008; 0.282028±34). The mass-bias correction considered the signal of ^{171}Yb and ^{173}Yb and, additionally, these isotopes, as well as ^{175}Lu, were applied in the isobaric interference correction of Yb and Lu on the ^{176}Hf signal. The studied zircon grains show very low Lu/Hf values (<0.0004), which reflect that the primary Hf isotopic composition is preserved and, consequently, no overcorrection is needed. Calculation of ε_{Hf} and T_{DM} model ages for each single spot analyses were based on the $^{206}Pb/^{238}U$ age, previously determined in the same grain. Errors for isotopic ratios are presented at the 2σ level.

Ion microprobe analyses were carried out in one sample using SHRIMP I at the Research School of Earth Sciences, Australian National University, Canberra, Australia. Data were collected and reduced as described by Williams & Claesson (1987) and Compston (1992). Uncertainties are given at 1σ level, and final age quoted at 95% confidence level. Reduction of raw data was carried out using Squid 1.02 (Ludwig, 2001). U/Pb isotopic ratios were referenced to the RSES standard zircon AS3 (1099 Ma, $^{*206}Pb/^{238}U = 0.1859$, Paces & Miller (1993). U and Th concentrations were determined relative to those measured in the RSES standard SL13.

ID-TIMS analyses

For the conventional U-Pb analyses, fractions were dissolved in concentrated HF and HNO_3 (HF:HNO_3 = 4:1) using microcapsules in Parr-type bombs. A mixed ^{205}Pb-^{235}U spike was used. Chemical extraction followed standard anion exchange technique, using Teflon microcolumns, following modified procedures from Krogh (1973). Pb and U were loaded together on single Re filaments with H_3PO_4 and Si gel, and isotopic analyses were carried out on a Finnigan MAT-262 multi-collector mass spectrometer equipped with secondary electron multiplier-ion counting, at the Geochronology Laboratory of the University of Brasília. Procedure blanks for Pb, at the time of analyses, were better than 20 pg. Data reduction and age calculations were performed using the PBDAT (Ludwig, 1993) and ISOPLOT version 3.0 (Ludwig, 2003) software. Errors for isotopic ratios are quoted at 2σ.

Sm-Nd isotopic analyses followed the method described by Gioia & Pimentel (2000) and were carried out at the Geochronology Laboratory of the University of Brasília. Whole rock powders (ca. 50 mg) were mixed with ^{149}Sm-^{150}Nd spike solution and dissolved in Savillex capsules. Sm and Nd extraction of whole-rock samples followed conventional cation exchange techniques. Sm and Nd samples were loaded on Re evaporation filaments of double filament assemblies and the isotopic measurements were carried out on a multi-collector Finnigan MAT 262 mass spectrometer in static mode. Uncertainties for Sm/Nd and $^{143}Nd/^{144}Nd$ ratios are better than ±0.5% (2σ) and ±0.005% (2σ), respectively, based on repeated analyses of international rock standards BHVO-1 and BCR-1. The $^{143}Nd/^{144}Nd$ ratios were normalized to $^{146}Nd/^{144}Nd$ of 0.7219 and the decay constant used was 6.54×10^{-12} a^{-1}. The T_{DM} values were calculated using the model of DePaolo (1981). Nd procedure blanks were better than 100 pg.

3.5. Samples and results

Damolândia region

Sample DM-16 is a leucogabbro corresponding to a residual, late-stage influx of magma that cut across other partially crystallized rocks. The analyzed drill-core sample from the Damolândia Layered Complex corresponds to a heterogeneous interval in terms of metamorphism, in which strongly deformed and metamorphosed areas with polygonal mineral boundaries co-exist with relict igneous pyroxene grains (see Figure 3.2 for location).

Zircon crystals occur either within adcumulate phases or within plagioclase and hornblende crystals. They are commonly bordered by intergrowths of ilmenite and magnetite. Zircon crystals are pristine, colorless to pink and show stubby to prismatic habit with varied degrees of rounding. Generally, grains are fragmented and their widths vary between 300 and 800 μm. Under cathodoluminescence, they show well defined sector zoning and are surrounded by a thin, bright outer rim with irregular boundaries (Figure 3.10A). Zircon usually contains inclusions of apatite, pyrite and ilmenite, around which recrystallization also occurs.

Eighteen U-Pb spot analyses render a chain of concordant ages spreading from 670 Ma down to 590 Ma (Figure 3.11A). There is no obvious correlation between internal structure of the crystal and U-Pb data, since there are grains with similar ages (within error) in both rim and core (Table 3.1). Lu-Hf analyses reveal $^{176}Hf/^{177}Hf_{ap}$ ratios between 0.282119 to 0.282290, and strongly negative $\varepsilon_{Hf(T)}$ signature, ranging from -3.06 to -9.83 (Table 3.2). Two-stage hafnium model ages yield $T_{(DM)}$ values from 1.60 to 1.93 Ga.

Nd isotopic data obtained for the Damolândia Layered Complex render Nd model ages between 1.78 and 2.16 Ga, with strongly negative ε_{Nd} (T=650 Ma) values (-3.9 to -26.5) (Table 3.3). The Sm-Nd data, plotted against the stratigraphy of the drill hole FSDM-07, reveals that the ε_{Nd} variation is related merely to different degrees of assimilation during the emplacement in an older continental crust (Figure 3.4).

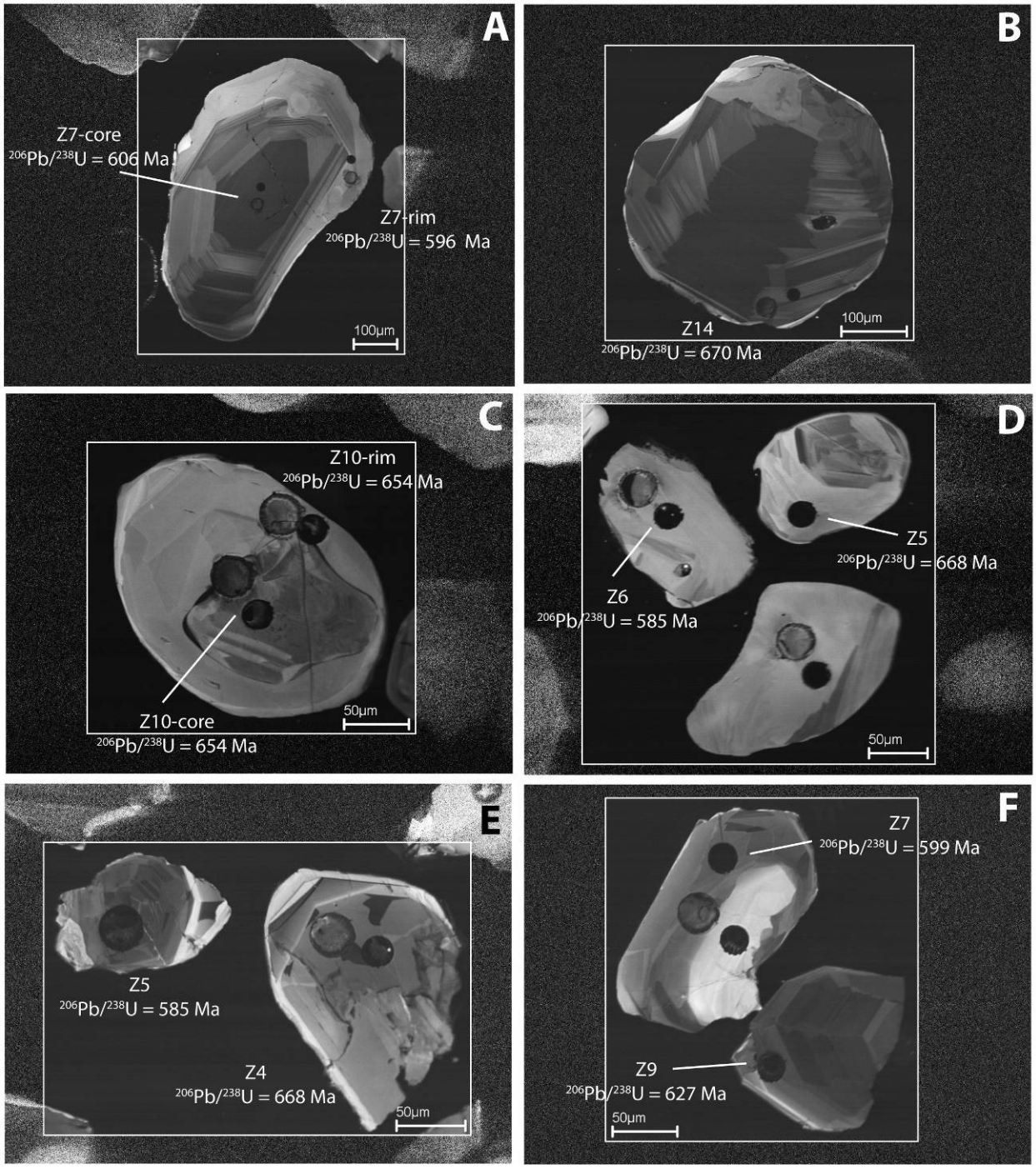

Figure 3.10 – CL images of zircon from sample DM-16 (A, B), sample DM-20 (C, D) and sample TQ-14 (E, F). Smaller spots (30 µm) represent the location of U-Pb analyses, whereas larger spots (40 µm) correspond to Hf isotopic investigation.

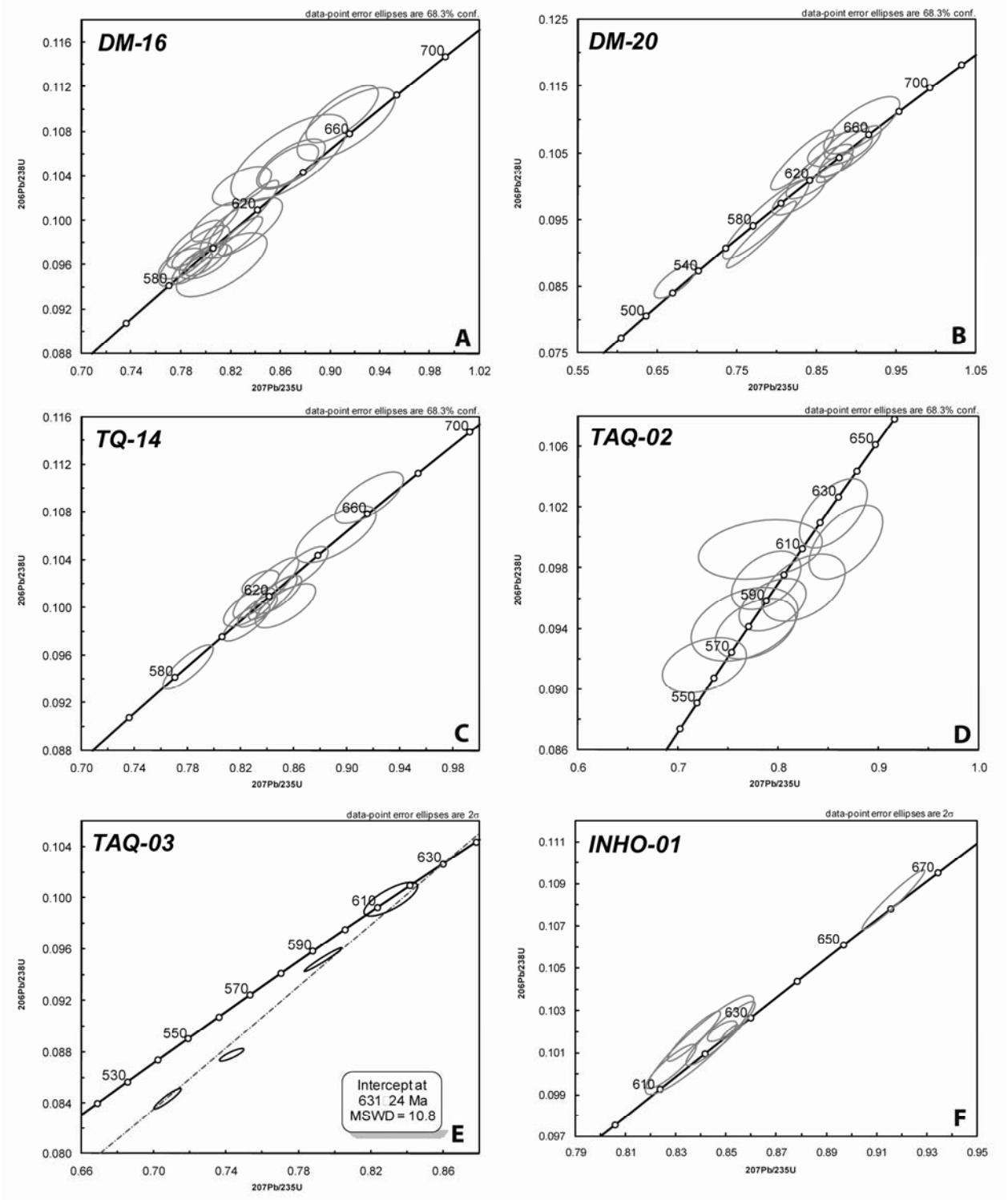

Figure 3.11 - LA-ICPMS (A-C), SHRIMP (D) and ID-TIMS (E-F) U-Pb plots for Damolândia (DM), Taquaral (TQ, TAQ) and Goianira-Trindade complexes (INHO).

Table 3.1 – U-Pb LA-ICPMS data for sample DM-16.

Sample	f(206) %	Th/ U	6/4 ratio	7/6 ratio	1s (%)	7/5 ratio	1s (%)	6/8 ratio	1s (%)	Apparent ages						Rho	Conc (%)
										7/6 age	1σ	7/5 age	1σ	6/8 age	1σ		
004-Z1	0.19	0.26	11848	0.05912	1.1	0.7891	1.4	0.09680	0.9	571.6	23.5	590.6	6.2	595.6	4.9	0.61	104
005-Z2	0.11	0.20	15807	0.06020	1.3	0.7996	1.7	0.09633	1.1	610.8	29.0	596.6	7.8	592.9	6.1	0.62	97
008-Z3	0.62	0.22	2884	0.05863	1.2	0.7915	1.9	0.09791	1.4	553.3	26.9	592.0	8.5	602.2	8.3	0.76	109
009-Z4	0.20	0.16	11349	0.05887	1.2	0.7803	1.5	0.09613	1.0	562.3	26.4	585.6	6.9	591.7	5.4	0.61	105
010-Z5	0.23	0.19	7649	0.06010	0.9	0.8000	1.4	0.09654	1.0	607.2	20.4	596.8	6.3	594.1	5.9	0.74	98
011-Z6	0.21	0.18	8499	0.06046	1.9	0.8283	2.7	0.09937	1.8	619.9	41.8	612.6	12.2	610.7	10.6	0.72	99
014-Z7RIM	0.32	0.21	5512	0.05920	1.4	0.7904	2.4	0.09683	1.9	574.5	30.7	591.4	10.6	595.8	10.7	0.80	104
015-Z7-CORE	0.12	0.27	14087	0.06089	0.8	0.8278	1.4	0.09861	1.2	635.3	17.1	612.4	6.6	606.2	6.9	0.84	95
016-Z8	0.09	0.20	18741	0.05973	0.9	0.7888	1.4	0.09578	1.0	593.8	19.9	590.5	6.1	589.6	5.7	0.75	99
017-Z9	0.14	0.18	13115	0.06138	2.2	0.8127	3.0	0.09602	2.0	652.6	47.8	604.0	13.5	591.1	11.1	0.68	91
021-Z10	0.09	0.20	19111	0.05861	1.0	0.8070	1.5	0.09986	1.2	552.7	21.9	600.8	7.0	613.6	6.8	0.76	111
022-Z11	0.14	0.20	2190	0.05993	1.5	0.8683	2.1	0.10508	1.4	601.2	33.1	634.7	9.8	644.1	8.7	0.68	107
023-Z12	0.11	0.25	16144	0.05832	1.5	0.8291	1.9	0.10311	1.1	541.6	33.4	613.1	8.7	632.6	6.7	0.58	117
024-Z13	0.12	0.18	14238	0.05951	2.6	0.8667	3.6	0.10563	2.4	585.7	56.9	633.8	16.9	647.3	15.0	0.69	111
027-Z14	0.25	0.18	7118	0.06020	1.4	0.9093	2.1	0.10955	1.5	610.8	31.3	656.7	10.2	670.1	9.8	0.73	110
028-Z15	0.18	0.20	8927	0.05989	1.4	0.8665	1.8	0.10494	1.2	599.5	29.3	633.7	8.6	643.3	7.5	0.67	107
029-Z16	0.27	0.29	6526	0.05986	1.0	0.8300	2.2	0.10056	2.0	598.5	21.0	613.6	10.4	617.7	12.0	0.91	103
030-Z17	0.20	0.32	8744	0.06093	2.1	0.9129	2.9	0.10866	2.0	636.9	44.3	658.6	13.8	665.0	12.5	0.71	104

Table 3.2 - Summary of in situ Lu–Hf analyses for sample DM-16.

Sample	176Lu/177Hf	2σ	176Hf/177Hf	2σ	Age (Ma)	(176Hf/177Hf)t	2σ	eHf(t)	1σ	$T_{(DM)}$ (Ga)
003-Z1	0.0004016	±0.000005	0.282129	0.000025	596	0.282124	0.000025	-9.83	±0.40	1.93
004-Z2	0.0004241	±0.000000	0.282198	0.000030	593	0.282193	0.000030	-7.47	±0.55	1.80
005-Z7-RIM	0.0003607	±0.000002	0.282236	0.000025	596	0.282232	0.000025	-6.03	±0.39	1.73
006-Z7-CORE	0.0006237	±0.000003	0.282159	0.000029	606	0.282152	0.000029	-8.63	±0.51	1.88
009-Z6	0.0002894	±0.000002	0.282229	0.000026	611	0.282226	0.000026	-5.92	±0.40	1.73
010-Z11	0.0003603	±0.000001	0.282290	0.000038	644	0.282285	0.000038	-3.07	±0.82	1.60
011-Z12	0.0004843	±0.000001	0.282193	0.000028	633	0.282187	0.000028	-6.79	±0.47	1.80
012-Z13	0.0003522	±0.000000	0.282156	0.000034	647	0.282151	0.000034	-7.74	±0.67	1.86
015-Z15	0.0003595	±0.000000	0.282123	0.000038	643	0.282119	0.000038	-8.98	±0.80	1.92
016-Z14	0.0004665	±0.000004	0.282195	0.000036	670	0.282189	0.000036	-5.91	±0.72	1.78
017-Z4	0.0005511	±0.000003	0.282231	0.000023	592	0.282225	0.000023	-6.36	±0.34	1.74
018-Z5	0.0003581	±0.000002	0.282220	0.000025	594	0.282216	0.000025	-6.64	±0.39	1.76

Table 3.3 - Sm-Nd data for the Damolândia Complex.

Sample	Lithotype	Prof. (m)	Sm(ppm)	Nd(ppm)	$^{147}Sm/^{144}Nd$	$^{143}Nd/^{144}Nd$	$(^{143}Nd/^{144}Nd)i$	$\varepsilon_{(0)}$	$\varepsilon_{(T)}$	T_{CHUR}(Ma)	T_{DM}(Ma)
DM 01	Gabbro	283.0	2.3296	9.4894	0.1484	0.512159	0.511527	-9.34	-5.34	1503	2046
DM 02	Gabbro	282.4	2.5896	11.0190	0.1421	0.512162	0.511557	-9.29	-4.75	1321	1857
DM 03	Norite	280.9	1.7779	7.8426	0.1370	0.511029	0.510445	-31.39	-26.48	-	-
DM 04	Norite	276.4	1.7122	7.2050	0.1437	0.512083	0.511471	-10.82	-6.43	1585	2073
DM 05	Norite	241.5	1.8431	6.5716	0.1695	0.512323	0.511601	-6.14	-3.89	-	-
DM 07	Orthopyroxenite	217.8	0.6952	2.4391	0.1723	0.512198	0.511464	-8.58	-6.56	-	-
DM 08	Orthopyroxenite	216.0	0.8166	2.8761	0.1716	0.512303	0.511572	-6.53	-4.45	-	-
DM 10	Pyroxenite	209.4	4.1570	15.6256	0.1608	0.512360	0.511675	-5.42	-2.44	1171	1947
DM 14	Ol-Orthopyroxenite	102.2	0.4490	1.7858	0.1520	0.512162	0.511514	-9.29	-5.59	1614	2162
DM 15	Orthopyroxenite	99.3	0.7883	2.5250	0.1887	0.512024	0.511220	-11.98	-11.33	-	-
DM-16	Gabbronorite	68.0	4.6482	27.7413	0.1013	0.511722	0.511290	-17.88	-9.96	1458	1778
DM 18	Mafic granulite		18.7812	105.0402	0.1081	0.512223	0.511763	-8.09	-0.72	710	1176
DM 20	Mafic granulite		3.8743	12.3038	0.1903	0.512642	0.511831	0.09	0.61	-	-

Table 3.4 - U-Pb LA-ICPMS data for sample DM-20.

Sample	f(206) %	Th/ U	6/4 ratio	7/6 ratio	1s (%)	7/5 ratio	1s (%)	6/8 ratio	1s (%)	Apparent ages 7/6 age	1σ	7/5 age	1σ	6/8 age	1σ	Rho	Conc (%)
005-Z2	0.65	0.13	2747	0.05679	1.7	0.6721	2.6	0.08583	2.0	483.4	38.5	522.0	10.7	530.8	9.9	0.75	110
013-z5	0.48	-0.02	3677	0.06019	2.3	0.9064	3.5	0.10923	2.6	610.3	49.9	655.1	16.7	668.2	16.3	0.75	110
014-z6	0.37	0.24	4609	0.05997	1.9	0.7862	4.5	0.09508	4.1	602.6	41.6	589.0	20.3	585.5	23.0	0.91	97
016-z8	0.23	0.25	7620	0.06054	1.9	0.8538	3.3	0.10229	2.6	623.0	41.3	626.8	15.3	627.8	15.8	0.82	101
021-z10-rim	0.34	0.14	5251	0.06141	1.6	0.8916	2.9	0.10530	2.4	653.7	34.7	647.2	13.9	645.4	14.8	0.83	99
022-z10-core	0.24	0.04	8689	0.06034	1.4	0.8875	2.1	0.10668	1.6	615.7	29.7	645.1	10.0	653.5	9.8	0.75	106
023-z11	0.33	0.19	5444	0.06138	2.0	0.8736	1.7	0.10322	1.2	652.7	42.9	637.5	7.8	633.2	7.1	0.72	97
028-z14	0.32	0.00	5792	0.06078	3.3	0.8270	2.7	0.09868	2.0	631.5	69.7	611.9	12.1	606.7	11.4	0.75	96
029-z15	0.12	0.03	14547	0.06154	0.8	0.8663	1.3	0.10209	1.0	658.3	17.8	633.6	6.0	626.7	5.8	0.77	95
030-z16	0.14	0.00	12996	0.06034	2.5	0.8792	3.0	0.10567	1.6	616.0	54.9	640.6	14.4	647.6	10.2	0.56	105
025-z19	0.30	0.16	5757	0.05805	1.5	0.8322	3.2	0.10397	2.8	531.7	31.9	614.8	14.6	637.6	17.1	0.89	120

Table 3.5 - Summary of in situ Lu–Hf analyses for sample DM-20.

Sample	176Lu/177Hf	2σ	176Hf/177Hf	2σ	Age (Ma)	(176Hf/177Hf)t	2σ	eHf(t)	1σ	$T_{(DM)}$ (Ga)
003-Z6	0.0003607	±0.000001	0.282587	0.000029	586	0.282583	0.000029	6.19	±0.53	1.04
005-Z8	0.0005757	±0.000001	0.282421	0.000046	628	0.282414	0.000046	1.14	±1.09	1.35
006-Z20	0.0001376	±0.000001	0.282375	0.000051	580	0.282373	0.000051	-1.36	±1.31	1.46
009-Z10-CORE	0.0000417	±0.000002	0.282447	0.000031	645	0.282447	0.000031	2.69	±0.57	1.28
010-Z10-RIM	0.0001762	±0.000004	0.282511	0.000042	654	0.282508	0.000042	5.04	±0.95	1.16
011-Z14	0.0000732	±0.000001	0.282292	0.000060	606	0.282291	0.000060	-3.70	±1.64	1.61
012-Z15	0.0001804	±0.000001	0.282519	0.000063	627	0.282517	0.000063	4.74	±1.71	1.15

Table 3.6 - U-Pb LA-ICPMS data for sample TQ-14.

Sample	f(206) %	Th/ U	6/4 ratio	7/6 ratio	1s (%)	7/5 ratio	1s (%)	6/8 ratio	1s (%)	Apparent ages						Rho	Conc (%)
										7/6 age	1σ	7/5 age	1σ	6/8 age	1σ		
005-Z2	0.14	0.02	12260	0.05993	1.1	0.8269	1.6	0.10007	1.1	600.9	24.9	611.9	7.2	614.8	6.3	0.68	102
007-Z4	0.17	0.00	10215	0.06088	1.3	0.9169	1.9	0.10922	1.3	635.1	28.4	660.7	9.0	668.2	8.3	0.70	105
010-Z5	0.11	0.05	15679	0.05954	0.9	0.7801	1.6	0.09502	1.3	587.0	20.3	585.5	7.1	585.2	7.3	0.82	100
012-Z7	0.19	0.01	9530	0.05859	1.0	0.7865	1.4	0.09737	0.9	551.8	22.2	589.2	6.0	599.0	5.1	0.65	109
016-Z9	0.10	0.07	17716	0.05928	0.9	0.8346	1.1	0.10212	0.7	577.2	18.9	616.2	5.0	626.8	3.9	0.58	109
018-Z11	0.13	0.03	14002	0.06053	0.8	0.8324	1.2	0.09973	0.9	622.7	17.2	614.9	5.5	612.8	5.2	0.75	98
022-Z13	0.12	0.03	15039	0.06085	0.9	0.8482	1.4	0.10110	1.0	633.9	19.6	623.7	6.4	620.9	6.2	0.76	98
023-Z14	0.11	0.00	21400	0.06051	0.9	0.8243	1.4	0.09880	1.1	621.8	19.4	610.4	6.5	607.4	6.3	0.78	98
024-Z15	0.08	0.03	23582	0.06070	0.8	0.8442	1.5	0.10087	1.2	628.6	17.1	621.5	6.7	619.5	7.2	0.85	99
025-Z16	0.08	0.07	22193	0.06092	1.7	0.8917	2.2	0.10616	1.5	636.4	35.6	647.3	10.6	650.4	9.2	0.68	102
028-Z17	0.12	0.00	14569	0.05986	1.0	0.8390	1.9	0.10165	1.6	598.5	22.5	618.6	9.0	624.1	9.8	0.85	104
029-Z18	0.13	0.04	13054	0.06080	1.0	0.8661	1.5	0.10332	1.1	632.1	21.3	633.4	7.1	633.8	6.9	0.76	100
030-Z19	0.25	0.00	7064	0.06181	1.3	0.8536	1.7	0.10016	1.2	667.4	26.9	626.6	8.2	615.4	7.1	0.69	92

Table 3.7 - Summary of in situ Lu–Hf analyses for sample TQ-14.

Sample	176Lu/177Hf	2σ	176Hf/177Hf	2σ	Age	(176Hf/177Hf)t	2σ	eHf(t)	1σ	T(DM) Ga
004-Z2	0.0001583	±0.000003	0.282301	0.000065	615	0.282299	0.000065	-3.19	±1.80	1.59
005-Z4	0.0000923	±0.000001	0.282287	0.000040	668	0.282286	0.000040	-2.47	±0.85	1.59
006-Z5	0.0002344	±0.000004	0.282343	0.000064	585	0.282341	0.000064	-2.34	±1.78	1.52
009-Z7	0.0002078	±0.000001	0.282200	0.000073	599	0.282197	0.000073	-7.03	±2.08	1.79
011-Z11	0.0002111	±0.000012	0.282267	0.000057	612	0.282265	0.000057	-4.51	±1.50	1.65
012-Z14	0.0002436	±0.000005	0.282249	0.000039	607	0.282247	0.000039	-5.25	±0.87	1.69
013-Z15	0.0002784	±0.000006	0.282338	0.000049	619	0.282335	0.000049	-1.86	±1.21	1.51
014-Z16	0.0001586	±0.000002	0.282255	0.000048	650	0.282252	0.000048	-4.09	±1.15	1.66

Table 3.8 - U-Pb SHRIMP data for sample TAQ-02.

Grain spot	% 206 Pb	U ppm	Th ppm	232Th/ 238U	ppm 206Pb*	6/8 age	7/6 age	Conc (%)	207/206 ratio	±%	207/235 ratio	±%	206/238 ratio	±%	err corr
1.1	0.00	96	55	0.59	7.03	525.0 ±6.3	633 ± 39	17	0.0608	1.8	0.712	2.2	0.0848	1.3	0.57
2.1	0.50	65	30	0.48	5.15	565.3 ±7.3	510 ± 77	-11	0.0575	3.5	0.726	3.8	0.0916	1.3	0.36
3.1	0.42	32	16	0.52	2.60	581.1 ±9.4	564 ± 94	-3	0.0589	4.3	0.766	4.6	0.0943	1.7	0.76
4.1	0.00	38	17	0.47	3.26	612.9 ±9.1	709 ± 51	14	0.0630	2.4	0.867	2.8	0.0997	1.6	0.55
5.1	0.56	62	27	0.45	5.31	609.8 ±7.7	498 ± 110	-22	0.0572	5.1	0.782	5.2	0.0992	1.3	0.25
6.1	0.00	47	30	0.65	4.07	623.6 ±8.7	640 ± 47	3	0.0610	2.2	0.855	2.6	0.1016	1.5	0.56
7.1	0.32	55	25	0.47	4.47	579.4 ±7.5	600 ± 68	3	0.0599	3.1	0.777	3.4	0.0940	1.4	0.40
8.1	0.27	46	22	0.51	3.81	594.8 ±8.4	671 ± 64	11	0.0619	3.0	0.925	3.3	0.0967	1.5	0.44
9.1	0.25	68	36	0.55	5.72	598.1 ±7.3	559 ± 56	-7	0.0588	2.6	0.788	2.9	0.0972	1.3	0.44
10.1	0.27	71	59	0.87	5.81	588.4 ±7.0	612 ± 55	4	0.0602	2.5	0.794	2.8	0.0956	1.2	0.44

Table 3.9 – U-Pb ID-TIMS data for sample TAQ-03.

								Radiogenic Ratios							Age			
Sample	# grains	Size (mg)	U ppm	Th ppm	Pb ppm	U/ Th	206/ 204	207*/ 235		206* /238		rho	207*/ 206*		206*/ 238	207*/ 235	207*/ 206*	Ma
TAQ03R	1	0.019	416.29	57.27	38.216	7.27	635	0.7073	0.89	0.0844	0.78	0.932	0.0608	0.23	522	543	632	9
TAQ03S	1	0.02	186.31	54.41	36.839	3.42	76	0.8305	1.45	0.0999	1.09	0.757	0.0609	0.8	608	614	636	36
TAQ03T	2	0.034	303.7	32.01	30.012	9.49	668	0.7428	0.74	0.0878	0.43	0.854	0.0614	0.21	542	564	653	11
TAQ03U	3	0.025	199.65	43.53	20.996	4.59	555	0.7932	1.09	0.0952	0.8	0.976	0.0604	0.21	586	593	620	7

Table 3.10 – Sm-Nd data for the Taquaral Complex.

Sample	Lithotype	Prof. (m)	Sm(ppm)	Nd(ppm)	$^{147}Sm/^{144}Nd$	$^{143}Nd/^{144}Nd$	$(^{143}Nd/^{144}Nd)i$	$\varepsilon_{(0)}$	$\varepsilon_{(T)}$	T_{CHUR}(Ma)	T_{DM}(Ma)
TQ 03	Gabbronorite	33.4	2.144	7.858	0.1649	0.512306	0.511603	-6.48	-3.85	1581	2293
TQ 05	Gabbronorite	55.2	7.981	29.540	0.1633	0.512238	0.511542	-7.81	-5.05	1814	2432
TQ 06	Orthopyroxenite	65.7	1.324	3.050	0.2624	0.512538	0.511420	-1.95	-7.42	-	-
TQ 08	Orthopyroxenite	83.6	2.121	8.847	0.1449	0.512424	0.511806	-4.18	0.12	626	1358
TQ 10	Gabbronorite	120.7	3.646	13.196	0.1670	0.512445	0.511733	-3.77	-1.31	982	1930
TQ 12	Gabbronorite	136.5	4.155	13.688	0.1835	0.512643	0.511862	0.11	1.21	-	-
TQ 15	Orthopyroxenite	173.0	0.638	1.200	0.3212	0.512547	0.511179	-1.78	-12.14	-	-
TQ 16	Gabbronorite	183.2	3.136	7.586	0.2499	0.513232	0.512168	11.59	7.18	-	-
TQ 18	Peridotite	198.4	0.099	0.189	0.3162	0.512773	0.511426	2.64	-7.31	-	-
TQ 22	Mafic granulite		5.893	22.327	0.1596	0.512354	0.511674	-5.54	-2.46	1157	1919

Table 3.11 – U-Pb ID-TIMS data for sample INHO-01.

									Radiogenic Ratios					Age			
Sample	# grains	Size (mg)	U ppm	Th ppm	Pb ppm	U/ Th	206/ 204	207*/ 235	206* /238			rho	207*/ 206*		206*/ 238	207*/ 235	207*/ 206*	Ma
INHO7	3	0.022	566.71	57.345	49.46	0.09	3573	0.8484	0.56	0.1020	0.383	0.73	0.0603	0.386	626	624	614	8.3
INHO10	1	0.012	993.29	102.08	90.68	0.09	3536	0.8513	0.32	0.1020	0.296	0.91	0.0605	0.132	626	625	623	2.8
INHO8	5	0.017	94.138	11.537	64.01	0.68	483	0.9168	1.11	0.1083	1.07	0.96	0.0614	0.289	663	661	654	6.2
INHO2	4	0.026	140.52	15.063	41.85	0.30	928	0.8477	1.33	0.1019	1.22	0.92	0.0603	0.516	625	623	616	11
INHO5	4	0.026	147.74	16.077	41.85	0.28	880	0.8371	1.04	0.1018	0.949	0.93	0.0596	0.386	635	618	591	8.4
INHO13	3	0.015	601.99	65.572	72.55	0.12	851	0.8281	0.98	0.1003	0.85	0.88	0.0598	0.465	616	613	598	10
INHO14	2	0.019	201.34	22.302	57.27	0.28	368	0.8395	2.11	0.1014	1.9	0.91	0.0600	0.864	622	619	606	19

Table 3.12 - Sm-Nd data for the Goianira-Trindade Complex.

Sample	Sm(ppm)	Nd(ppm)	$^{147}Sm/^{144}Nd$	$^{143}Nd/^{144}Nd$	$(^{143}Nd/^{144}Nd)i$	$\varepsilon_{(0)}$	$\varepsilon_{(T)}$	T_{CHUR}(Ma)	T_{DM}(Ma)
GT-4	1.517	4.121	0.223	0.512772	0.511822	2.61	0.43	789	-
GT-6B	3.91	10.68	0.221	0.512748	0.511807	2.15	0.13	703	-
GT-6C	1.663	4.988	0.202	0.512711	0.511850	1.42	0.99	2149	-
GT-9A	2.705	8.329	0.196	0.512648	0.511813	0.20	0.25	-	-
GT-9B	0.881	4.785	0.111	0.5123	0.511827	-6.59	0.53	-	1098
GT-9D	4.833	13.7	0.213	0.512719	0.511812	1.58	0.23	777	-
GT-10B	4.349	12.54	0.21	0.512647	0.511752	0.18	-0.93	-	-
GT-41	0.133	0.463	0.174	0.512704	0.511963	1.29	3.18	-	1281

Sample DM-20 corresponds to a strongly foliated mafic granulite with dioritic composition, exposed near (~2.5 km) an occurrence of sapphirine+quartz bearing granulites (sample PT-62; Moraes *et al.*, 2002; Baldwin *et al.*, 2005). In sample DM 20, zircon is included in plagioclase crystals and also occurs close to hornblende corona. Zircon grains are approximately 150 μm long and are pristine and colorless. Commonly, these crystals show a "soccer-ball" habit, with rounded terminations, typical of zircon grown under granulite facies conditions (Vavra *et al.*, 1999; Schaltegger *et al.*, 1999). Primary internal texture in igneous crystals is represented by sector zoning, which is partially preserved in some grains, while featureless zircon is the main metamorphic texture. Some grains also show bright, luminescent rims with lobate, curved inward boundaries (Figure 3.10B). Generally, these luminescent domains render highly discordant U-Pb ages.

Ten spot analyses yield a spread of concordant ages from 670 to 530 Ma (Figure 3.11B; Table 3.4) and identical ages in rims and cores are identified, similarly to the previously described results for sample DM-16. $^{176}Hf/^{177}Hf_{ap}$ ratios range from 0.282291 to 0.282583 and $\varepsilon_{Hf(T)}$ vary in the interval of 5.73 to -3.65. Two-stage hafnium model ages reveal values from 1.05 to 1.60 Ga (Table 3.5).

Regional granulites, contrary to the mafic-ultramafic complex, show younger Nd model ages (1.2 Ga) and only slightly negative ε_{Nd} (T=650 Ma) values (-0.72; Table 3.3). This might indicate either a different degree of assimilation of older continental crust or even that these rocks were generated from a distinct, more depleted magma source.

Taquaral area

TQ-14 is an amphibolite drill-core sample from the Taquaral Layered Complex. Zircon grains occur included in plagioclase and hornblende. They are pristine, colorless and commonly show stubby to prismatic habit, with sharp to rounded surfaces. The crystals vary in size from 200 μm to 500 μm. Bright, luminescent cores with weak sector zoning usually present very low Pb contents and reveal highly discordant and occasionally younger U-Pb ages than that observed in the correspondent rim. These nucleii are surrounded by a dark domain and some grains also have a very thin and brilliant external rim (Figure 3.10C). In addition, featureless zircon is recurrent.

Thirteen spot analyses reveal concordant ages varying from 670 to 585 Ma (Figure 3.11C, Table 3.6). As observed in the Damolândia Complex, the scatter of ages cannot be linked to internal features in zircon grains. Hf isotopic ratios of these crystals range from 0.282197 to 0.282341, with strongly negative $\varepsilon_{Hf(T)}$ values (from -1.86 to -7.03). Two-stage Hf model ages vary between 1.51 and 1.69 Ga (Table 3.7).

Sample TAQ-02 corresponds to a medium-grained gabbronorite with granoblastic texture. Zircon crystals are pristine and occur as stubby to prismatic grains, smaller than 300 μm, that usually are fragmented. BSE imaging reveals the existence of cores with relict sector zoning, which are surrounded by a bright, outer domain with curved, irregular boundaries (Figure 3.10D). Featureless crystals are also commonly observed. Ten SHRIMP spot analyses yield variable discordant results, with $^{206}Pb/^{238}U$ ages ranging from 623 Ma to 525 Ma (Figure 3.11 D; Table 3.8).

In the Taquaral Complex, Nd model ages are slightly younger (1.36 to 1.92 Ga) and ε_{Nd} (T=650Ma) varies from +0.1 to -7.8 (Table 3.9). The deviation in the ε_{Nd} value reflects varied degrees of crustal contamination, similarly to that described for the Damolândia Complex (Figure 3.8).

Sample TAQ-03 corresponds to a porphyritic biotite orthogneiss exposed in the western margin of the mafic complex. It consists of pink, clear elongated and prismatic (4:1) zircon grains. Inclusions or fractures are rare. Four zircon fractions were investigated by conventional ID-TIMS and yielded highly discordant compositions. However, the upper intercept age of 631 ± 24 Ma (MSWD=8.1, Figure 3.11E, Table 3.9) is interpreted as being representative of the igneous crystallization.

Goianira-Trindade Complex

The Goianira-Trindade Complex is an additional mafic-ultramafic complex that occurs within the AIC, to the south of the Damolândia layered body (see Figure 3.1B for location). It is composed of peridotite, pyroxenite and gabbronorite, with varied degrees of deformation and high-grade metamorphic imprint, similarly to that described in the Damolândia and Taquaral complexes.

Sample INHO-01 is a coarse-grained leucogabbro in which two zircon populations can be distinguished. Small, prismatic grains characterize the first group, whereas the second is

composed of colorless, rounded crystals with stubby habit, typical of metamorphic growth. However, there is no correlation among the data obtained and zircon population. ID-TIMS analyses of seven fractions reveal variably discordant results with a cluster of $^{206}Pb/^{238}U$ ages around 620 Ma, whereas one fraction yield a value of 662 Ma (Figure 3.11F, Table 3.11).

Nd isotopic data obtained for seven cogenetic rocks from the Goianira-Trindade Complex reveal positive to slightly negative ε_{Nd} values (-0.93 to +3.18) and T_{DM} Nd model ages between 1.10 and 1.28 Ga (Table 3.12). The results suggest derivation from a depleted mantle, with restricted crustal contribution.

3.6.Discussion

"Metamorphic" zircon and the meaning of the spread of concordant U-Pb ages

Zircon is a common mineral in almost all rock types and occurs in a wide range of environments, ranging from the Earth's surface to deeper crustal levels. Owing to its resilience, even in such extreme conditions, zircon allows the link between P-T paths and geological time. However, recent studies have shown that processes taking place during high-grade metamorphism affect the U-Pb isotopic signature of zircon.

In granulite facies, zircon may display two distinct behaviors as a response to the extraordinary pressure and temperature conditions. New zircon may grow either in the subsolidus state, due to the breakdown of Zr-bearing minerals in metamorphic reactions, or from a melt/fluid phase (Roberts & Fringers, 1997; Fraser *et al.*, 1997; Schaltegger *et al.*, 1999; Vavra *et al.*, 1999; Degeling *et al.*, 2001; Bingen *et al.*, 201; Rubatto, 2002; Ayers *et al.*, 2003; Whitehouse & Platt, 2003; Möller *et al.*, 2003; Rubatto & Hermann, 2007). Growth of new zircon results in the overgrowth of older grains or in the crystallization of a new population of individual crystals. In general, minerals generated under such conditions are pristine and small. Their external and internal patterns are variable, as they might form prisms with oscillatory zoning (Nÿstrom & Kriegsman, 2003), as well as equant, granoblastic crystals with "soccer ball" habit (Vavra *et al.*, 1999; Schaltegger *et al.*, 1999).

However, the new zircon commonly shows different geochemical signature compared to the protolith igneous grain, since it crystallizes in (i) a chemically distinct environment, or (ii) in equilibrium with other minerals, such as garnet and monazite, which can influence the partition

coefficient of important constituents of zircon (Bingen *et al.*, 2001; Rubatto, 2002; Rubatto & Hermann, 2007). Besides that, because of the complete opening of the isotopic system, their ages and isotope ratios are distinguishable from older crystals and, hence, newly grown zircon records younger geological events.

In a second hypothesis, zircon can ***re-equilibrate*** in the presence of a fluid or a melt phase (Schaltegger *et al.*, 1999; Vavra *et al.*, 1999; Ashwal *et al.*, 1999; Hoskin & Black, 2000; Corfu *et al.*, 2003; Martin *et al.*, 2008). Under CL images, crystals that have experienced such alteration show an irregular and diffuse, curved inward boundary, typical of consumption (Hoskin & Black, 2000; Corfu *et al.*, 2003; Geisler *et al.*, 2007). Occasionally, primary structures are partially preserved, rendering a "ghost" feature in the altered zone (Hoskin & Black, 2000).

In this scenario, if the crystal is radiation-damaged, the defects may enhance the diffusion of elements in zircon, promoting both the gain of common Pb and unusual cations (Ca, Al, Fe) and the loss of essential components, such as Zr, Si, Pb, Hf, REE and U (Schaltegger *et al.*, 1999; Vavra *et al.*, 1999; Geisler *et al.*, 2007). Consequently, the diffusion reaction usually yields discordant U-Pb analyses.

However, if zircon is crystalline, re-equilibrium occurs dynamically in a coupled dissolution-reprecipitation process, in which the system remains closed (or partially closed) for the main components (Ashwal *et al.*, 1999; Putnis, 2002; Tomaschek *et al.*, 2003; Geisler *et al.*, 2007; Martin *et al.*, 2008). If the equilibrium is not complete, the crystal retains part of the isotopic and geochemical information of the protolith grain. Accordingly to that, such zones shall yield intermediate ages between primary, igneous ages, and secondary, metamorphic or hydrothermal alteration and, therefore, their geological meaning may not be real (Mezger & Krogstad, 1997; Hoskin & Black, 2000; Möller *et al.*, 2002; Geisler *et al.*, 2007).

Since the Lu-Hf isotopic system is decoupled from U-Pb systematics during alteration, it has been used to solve geological events related to such recrystallization processes (Gerdes & Zeh, 2009). In contrast to CL imaging and chemical analysis, Hf isotopes allow verifying the number of zircon forming episodes, based on the fact that individuals formed within an isotopically homogeneous magmatic suite and/or in the same geological event shall yield similar initial Hf isotopic ratios (Nebel *et al.*, 2007; Gerdes & Zeh, 2009).

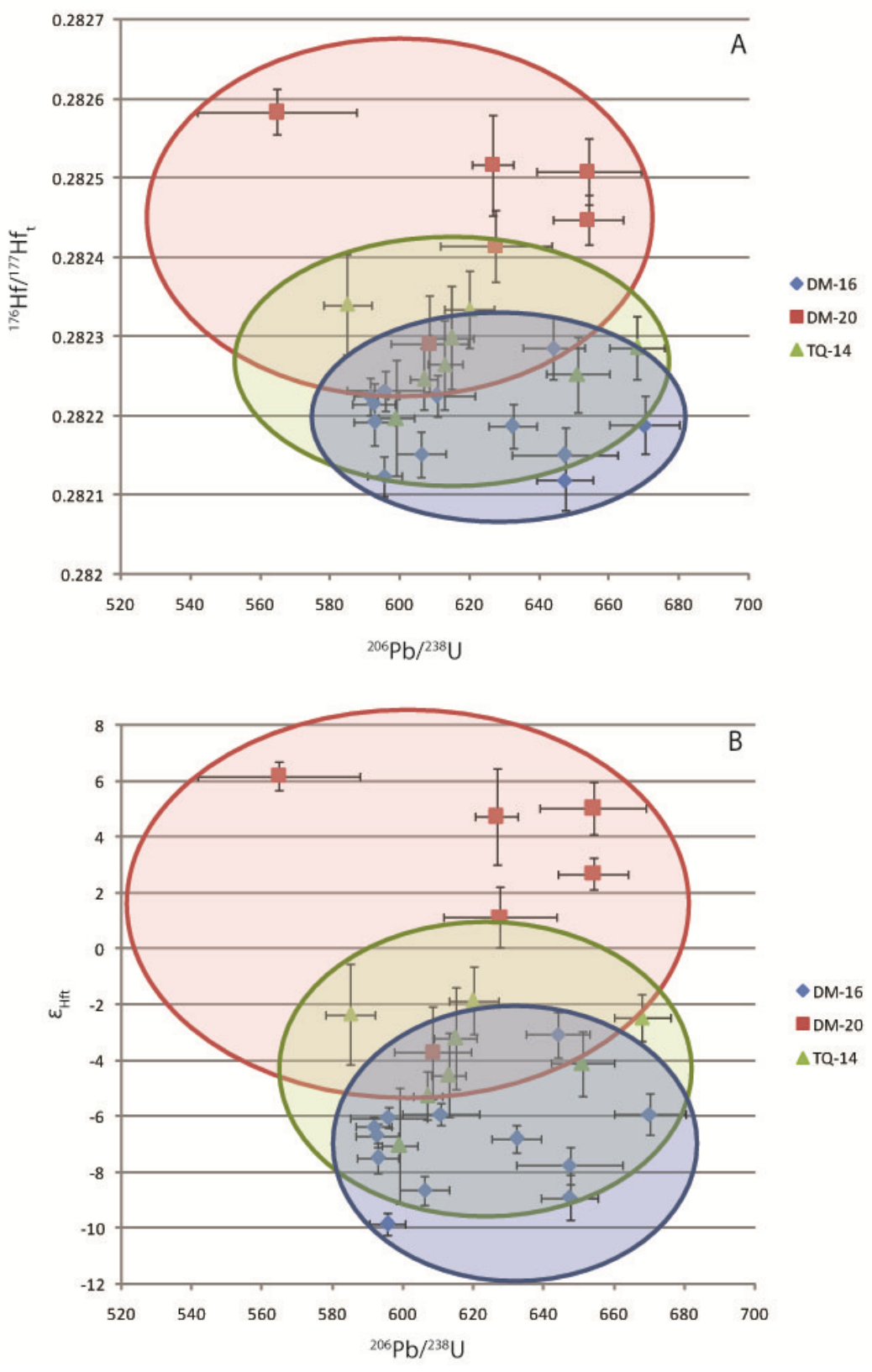

Figure 3.12 - Zircon i*n situ* Hf isotopic data (A, $^{176}Hf/^{177}Hf_t$; B, ε_{Hft}) versus U-Pb age plots.

As discussed in the previous section, there is a variation in the Hf isotopic signature of Damolândia and Taquaral zircon grains (Tables 3.2, 3.5 and 3.7). This behavior may be attributed to different degrees of interaction between mantle-derived melts and older crustal components, which is also corroborated by the Nd whole-rock data (Tables 3.3 and 3.10). However, neither the Hf isotopic ratios nor the $\varepsilon_{Hf}(t)$ can be linked to any specific zircon age domain. As shown in Figure 3.12, the Hf data scatter randomly along the $^{206}Pb/^{238}U$ axis, revealing no correlation with the large spread of concordant U-Pb ages, which suggests that the oscillation of Hf isotopic signature is related merely to crustal contamination and, therefore, all zircon crystals (within individual samples) were grown in a single geological episode.

As previously stated, since high-grade metamorphism does not disturb the Lu-Hf systematic in zircon grains, the Hf isotopic ratios should evidence primary, igneous conditions and, hence, the older ages, around 670 Ma, may be interpreted as representative of the emplacement of the Damolândia and Taquaral mafic-ultramafic complexes.

Furthermore, the Hf isotopic signature supports that, during metamorphism, in these complexes zircon ***re-equilibrated*** rather than ***re-grew***. This is also justified by the CL characteristics of the crystals, in which curved, inward-moving boundaries are frequent. The fact that all individuals reveal concordant ages and that there is no evidence of a radiation-damage effect in the analyzed grains suggests that crystals might have experienced a concomitant dissolution-reprecipitation process. In view of this, the observed chain of ages in the Concordia diagram probably corresponds to intermediate values between igneous crystallization and the final closure of the U-Pb isotopic system, following the high-grade metamorphism.

Nonetheless, it is still not possible to distinguish a clear peak metamorphic age for the studied rocks based only on zircon analyses. Further research on rutile and other metamorphic minerals is in progress and might help to elucidate this question in the future.

The geochronological framework here described is similar to that of the Napier Complex, Antarctica (Kelly & Harley, 2005) and, likewise, suggests that the studied rocks were kept in high temperatures for a long time. This unusually hot condition might be achieved in deep levels in the crust, where igneous crystallization and metamorphic overprint are concomitant. Moreover, it may promote the partial opening of the U-Pb system in zircon and, consequently, produce the large spread of ages observed in the AIC.

Comparison between dating methods

Another essential aspect when interpreting U-Pb data is the method used for dating. ID-TIMS ages are obtained from the dissolution of a randomly, optically selected grain and, occasionally, from more than one crystal. As stated in the previous section, zircon that undergoes re-equilibration during metamorphism might preserve a component of the original isotopic information. Therefore, the main issue remains on whether ID-TIMS ages of zircon crystals from metamorphic terranes have a geological meaning or are only a geochronological artifact enhanced by a memory effect. Moreover, obtaining the correct crystallization age might also depend on "luck" when picking the grains.

Such peculiarities may be shown in the sample INHO-01, in which U-Pb ID-TIMS analyses revealed a cluster of concordant to nearly concordant ages around 620 Ma, whereas only one fraction yielded a $^{206}Pb/^{238}U$ of 662 Ma (Table 3.11). The younger group of ages is analogous to other mafic-ultramafic complexes identified to the west of the AIC, in the domain of the Goiás Magmatic Arc (Laux *et al.*, 2004). Additionally, titanite grains of a wollastonite-scapolite marble that occurs nearby the Goianira-Trindade Complex rendered an age of 632 Ma (Moraes *et al.*, 2007).

Conversely, considering that re-equilibration of zircon grains during high-grade metamorphism was noteworthy in some of the mafic-ultramafic intrusions within the AIC and that the older value obtained in sample INHO-01 is similar to that interpreted as the crystallization age for both Damolândia and Taquaral rocks, it suggests an analogous geochronological framework for the three layered complexes.

However, it is not possible to confirm neither of the interpretations above based only in the available U-Pb ID-TIMS data and, therefore, this method has shown to be inadequate for dating high-grade metamorphic terranes such as the AIC.

In-situ dating methods such as SIMS and LA-ICPMS, for instance, have proven to be the more efficient technique in determining distinct geological events within one single grain, since it allows the analysis of all zircon domains, altered or not during metamorphism. Yet, the control of internal textures with CL or BSE imaging is a crucial condition for an accurate analysis and a correct interpretation of the ages obtained with these methods.

Tectonic implications for the evolution of the Brasília Belt

U-Pb zircon analyses of both Damolândia and Taquaral complexes revealed crystallization ages of ~ 670 Ma. Such values have been already reported in previous studies on the felsic high-grade rocks of the AIC (Piuzana *et al.*, 2003; Möller *et al.*, 2006). However, in such examples, older values were discarded as inheritance, rendering concordia ages of ca. 645 Ma, which are accepted as representative of the timing of high-grade metamorphism in the AIC (Piuzana *et al.*, 2003).

Nevertheless, Möller *et al.* (2006) also reported 680 Ma zircon cores in UHT paragranulites, which were interpreted as grown in a prograde path, in equilibrium with garnet. In addition, similar ages were obtained in rutile grains shielded in garnet, with Zr content that corresponds to peak temperatures (Möller *et al.*, 2006; Zack et.al., 2006). Therefore, the prograde metamorphism attested by the paragranulites suggests that the prograde-to-peak UHT stage in the AIC may have occurred around 680-670 Ma, earlier than previously suggested. If so, at least part of the widespread mafic magmatism is coeval with the high-grade metamorphic episode and most likely represents the additional heat source required to the development of the UHT assemblages.

The post-peak cooling age of the AIC is marked by the growth of euhedral individual zircon crystals in opx-bearing leucossome at ca. 630 Ma, as well as by the crystallization of titanite grains in wollastonite-scapolite marble (Möller *et al.*, 2006; Moraes *et al.*, 2007). Coeval to this stage are a number of mafic-ultramafic intrusions in the domain of the Goiás Magmatic Arc, with crystallization ages of ~630 Ma (Laux *et al.*, 2004).

Hence, there may have been two distinct episodes of mafic magmatism in the southern Brasília Belt; the older around 670 Ma and related to the development of the UHT assemblages and the latter, near 630 Ma, associated with the cooling history of the orogen.

The geological context here described, with voluminous mafic and felsic magmatism spatially and temporally associated with high-grade metamorphism, might correspond to extensional episodes within the collisional setting, during which the upwelling of the hot asthenosphere results in partial melting of both the mantle and continental crust generating extensive mafic and felsic magmatism.

3.7. Conclusions

Combined geological and new geochronological data on mafic rocks within the Anápolis-Itauçu Complex allow the following conclusions:

- The Damolândia and Taquaral intrusions correspond to layered mafic-ultramafic complexes, which partially preserve igneous textures, even with the pervasive, although heterogeneous, high-grade metamorphic overprint.
- Whole-rock Sm-Nd isotopic data attest the strongly contaminated signature of these mafic rocks, which indicates that they were emplaced into older continental crust.
- CL zircon images reveal internal textures typical of consumption, such as irregular, inward-moving boundaries, implying that these crystals were submitted to a varied degree of alteration during high-grade metamorphism.
- Hf-in-zircon analyses yield homogeneous isotopic ratios and ε_{Hf} values (within population) which cannot be linked to U-Pb ages, suggesting that the grains were crystallized in one single episode.
- In the studied rocks, during high-grade metamorphism zircon crystals have re-equilibrated rather than re-grew. Hence, the spread of ages between 670 and ~580 Ma illustrates that in such grains the U-Pb isotopic system was partially reset.
- From the statements above, it is concluded that the older ages, around 670 Ma, are representative of the igneous crystallization of the Damolândia and Taquaral complexes. Therefore, the studied rocks represent an older episode of mafic magmatism in the Brasília Belt than that recorded in the domain of the Goiás Magmatic Arc, to the west. However, the U-Pb data do not allow the discrimination of the peak metamorphic age.
- The mafic magmatism in the Brasília Belt is coeval to the prograde path of high-grade metamorphism and characterizes the additional heat source required for the development of UHT paragenesis in the paragranulites of the AIC.

3.8.Acknowledgments

Support from CNPq research grant (477347/2007-0) is thankfully acknowledged. M.M.P. and C.F.F.F. are CNPq research fellows. M.E.S.D.G. thanks CNPq fellowship. The authors are grateful to International Nickel Venture-INV and Amazônia Mineração for providing access to exploration data and support during field work. Horizonte Minerals and BCV Consultoria, which currently hold the mining rights for the Damolândia area, are also acknowledged. Sérgio Junges, Jeanne Grasyelle and Bárbara Lima are appreciated for providing laboratory assistance.